Biomacromolecules

Article

pubs.acs.org/Biomac

Degradable Ketal-Based Block Copolymer Nanoparticles for Anticancer Drug Delivery: A Systematic Evaluation

Benoit Louage,[†] Qilu Zhang,[‡] Nane Vanparijs,[†] Lenny Voorhaar,[‡] Sofie Vande Casteele,[§] Yang Shi,[∥] Wim E. Hennink,[∥] Jan Van Bocxlaer,[§] Richard Hoogenboom,*[,‡] and Bruno G. De Geest*[,†]

[†]Department of Pharmaceutics, Ghent University, Ottergemsesteenweg 460, 9000 Ghent, Belgium

[‡]Supramolecular Chemistry Group, Department of Organic and Macromolecular Chemistry, Ghent University, Krijgslaan 281 S4, 9000 Ghent, Belgium

[§]Department of Bioanalysis, Ghent University, Ottergemsesteenweg 460, 9000 Ghent, Belgium

[∥]Department of Pharmaceutics, Utrecht Institute for Pharmaceutical Sciences, Utrecht University, Universiteitsweg 99, 3584CG Utrecht, The Netherlands

Supporting Information

ABSTRACT: Low solubility of potent (anticancer) drugs is a major driving force for the development of noncytotoxic, stimuli-responsive nanocarriers, including systems based on amphiphilic block copolymers. In this regard, we investigated the potential of block copolymers based on 2-hydroxyethyl acrylate (HEA) and the acid-sensitive ketal-containing monomer (2,2-dimethyl-1,3-dioxolane-4-yl)methyl acrylate (DMDMA) to form responsive drug nanocarriers. Block copolymers were successfully synthesized by sequential reversible addition−fragmentation chain transfer (RAFT) polymerization, in which we combined a hydrophilic poly(HEA)$_x$ block with a (responsive) hydrophobic poly(HEA$_m$-*co*-DMDMA$_n$)$_y$ copolymer block. The DMDMA content of the hydrophobic block was systematically varied to investigate the influence of polymer design on physicochemical properties and in vitro biological performance. We found that a DMDMA content higher than 11 mol % is required for self-assembly behavior in aqueous medium. All particles showed colloidal stability in PBS at 37 °C for at least 4 days, with sizes ranging from 23 to 338 nm, proportional to the block copolymer DMDMA content. Under acidic conditions, the nanoparticles decomposed into soluble unimers, of which the decomposition rate was inversely proportional to the block copolymer DMDMA content. Flow cytometry and confocal microscopy showed dose-dependent, active in vitro cellular uptake of the particles loaded with hydrophobic octadecyl rhodamine B chloride (R18). The block copolymers showed no intrinsic in vitro cytotoxicity, while loaded with paclitaxel (PTX), a significant decrease in cell viability was observed comparable or better than the two commercial PTX nanoformulations Abraxane and Genexol-PM at equal PTX dose. This systematic approach evaluated and showed the potential of these block copolymers as nanocarriers for hydrophobic drugs.

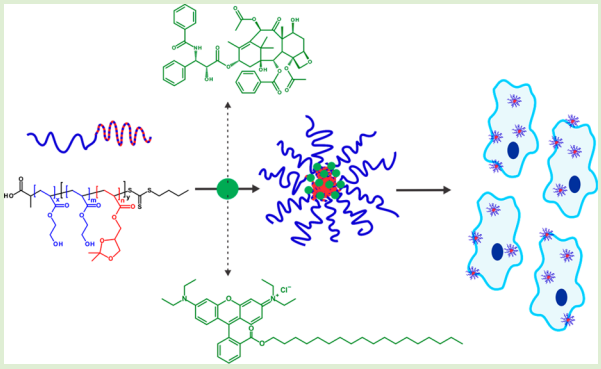

1. INTRODUCTION

Even though antineoplastic compounds with remarkable potential were already discovered half a century ago, poor solubility in aqueous medium still hampers widespread clinical use.[1,2] With a solubility of merely 0.3 μg/mL, paclitaxel (PTX), in particular, is considered as extremely hydrophobic.[3] PTX is an important anticancer drug, known for inhibiting cell replication by blocking microtubuli depolymerization during the late G2/M phase of the cell cycle. It has shown activity against several cancer types, including ovarian, lung, breast, bladder, neck, and AIDS-related Kaposi's sarcoma.[4,5] The clinically used PTX formulation, that is, Taxol, involves a 50:50 ethanol/Cremophor EL cosolvent mixture to enhance PTX solubility and allow systemic administration of a therapeutic relevant dose. However, severe side effects including anaphylactoid hypersensitivity reactions, hyperlipidaemia, abnormal lipoprotein patterns, aggregation of erythrocytes and peripheral neuropathy have been associated with Cremophor EL upon intravenous administration.[6] To avoid hypersensitivity, patients are pretreated with corticosteroids and antihistamines which, in turn, further complicates therapy and quality of life.[7]

Poor solubility and nonspecific pharmacodynamics of conventional chemotherapeutics have strongly contributed to an exponentially growing interest for advanced chemotherapy through nanoscale drug delivery systems.[8,9] Important assets have been ascribed to nanomedicines.[10,11] First, the use of alternative

Received: October 21, 2014
Revised: December 8, 2014
Published: December 9, 2014

Table 1. Block Copolymer Anti-Cancer Drug Delivery Systems in Clinical Trial[a]

formulation	block polymer type	diameter	drug	progress
Genexol-PM	mPEG−PDLLA	<50 nm	PTX	phase II[b]
NK-105	PEG−PAPB	85 nm	PTX	phase II
NK-012	PEG−PGlu-SN-38 conjugate	20 nm	SN-38	phase II
NK-911	PEG−PAsp-DOX conjugate	40 nm	DOX	phase II
NC-6004	PEG−PGlu	30 nm	cisplatin	phase I/II
NC-4016	PEG−PGlu	40 nm	oxaliplatin	phase I
BIND-014	PEG−PDLLA/PEG−PLGA	100 nm	docetaxel	phase I
SP-1049C	Pluronic L61, F127	30 nm	DOX	phase III

[a]Abbreviations: PDLLA, poly(D,L-lactide); PAPB, poly(aspartic acid) modified with 4-phenyl-butanol; PGlu, poly(glutamic acid); PAsp, poly(aspartic acid); PLGA, poly(D,L-lactic-*co*-glycolic acid); PTX, paclitaxel; SN-83, 7-ethyl-10-hydroxy-camptothecin; DOX, doxorubicin. [b]Approved in South Korea in 2007.

carriers can eliminate toxicity of excipients. Second, due to leaky vasculature and impaired lymphatic drainage, solid tumors have the tendency to retain nanoparticles especially when their size is below 200 nm.[12] This so-called enhanced permeability and retention (EPR) effect, along with prolonged circulation time, induced by the stealth corona on the surface of the nanoparticles as well as their larger size that reduces renal clearance, can lower the effective dose.[13,14] Third, drug solubility can be dramatically increased by encapsulation into hydrophobic compartments of nanovehicles. These assets have partly been confirmed in the clinic for Abraxane, an FDA-approved 130 nm albumin-stabilized (crystalline) paclitaxel formulation that is administered intravenously.[15] Compared to Taxol, it has reduced systemic toxicity and increased efficacy against several cancer types.[16] However, the manufacturing of nanocarriers containing recombinant proteins (i.e., human serum albumin in case of Abraxane) remains a costly process.[17]

Fully synthetic supramolecular polymeric nanostructures form a sound alternative for controlled drug delivery.[18] In particular nanoparticles composed of amphiphilic block copolymers (e.g., micelles, nanospheres and polymerosomes) have attracted increasing attention owing to their unique features, such as small size, high water-solubility, stability in the bloodstream, and high drug loading capacity, while they are generally well tolerated in vitro and in vivo.[19−21] In addition, amphiphilic block copolymers can be tailored in terms of responsiveness to external stimuli such as temperature, pH, enzymes, oxidation/reduction, and so on, allowing straightforward formulation strategies, selective drug release upon cellular uptake, and degradation in a biological medium.[22−26] Finally, the opportunity to engineer drug nanocarriers with targeting moieties enables active tumor targeting, which can be crucial in treating metastatic cancer.[27,28]

Amphiphilic block copolymers can be solid candidates for anticancer drug delivery, as several types already made it into clinical trials (Table 1).[29−33] Due to the promising potential of this technology, elaborate research has been conducted in the past decade to further fine-tune block copolymer properties. In this way, various pH- and temperature-responsive block copolymer systems have been reported in the literature.[34−37] The most widely described temperature-responsive polymeric systems are based on poly(*N*-isopropylacrylamide) (PNIPAM), poly(oligo(ethylene glycol)(meth)acrylate) (OEG(M)A), or poly(2-oxazoline) (POx), which exhibit a lower critical solution temperature (LCST) within the physiological relevant range in aqueous medium.[38−41] Reversible pH-sensitive systems have been developed using functional moieties of which the hydrophobicity is altered by protonation and deprotonation (e.g., tertiary amino groups).[42] In this way, Armes and co-workers reported on pH-sensitive vesicles based on a 2-(methacryloyloxy)ethyl phosphorylcholine (MPC) and 2-(diisopropylamino)ethyl methacrylate (DPA) diblock copolymer.[42] This system forms vesicles at pH > 6 and dissolves at lower pH values due to protonation of DPA, inducing a fast release of payload. A possible risk, however, of such reversible systems is bioaccumulation as reself-assembly can occur when the polymers exit acidic organelles (i.e., endosomes and lysosomes). This can be circumvented by using functional groups, which irreversibly switch into hydrophilic moieties under acidic conditions. Next to imines, hydrazides, hydrazones, orthoesters, and oximes, ketals are of particular interest due to their noncytotoxic nature.[43−48] Several pH-sensitive ketal-based polymeric structures have been reported (e.g., micelles and microparticles).[49,50] The irreversible hydrolysis of ketals at pH < 5 allows endosomal (pH 4−5.5) degradation and drug release. Furthermore, irreversible hydrolysis leads to fully soluble polymeric degradation products that should afford better (renal) clearance from the body.[51]

Reversible addition−fragmentation chain transfer (RAFT) polymerization has proven to be a powerful technique for the preparation of well-defined amphiphilic block copolymers.[52−54] Compared to other controlled radical polymerizations (CRP), such as nitroxide-mediated polymerization (NMP) and atom transfer radical polymerization (ATRP), RAFT polymerization excels in its versatility.[55−57] A wide variety of (functional) monomers can be prepared by RAFT polymerization in different solvents under mild reaction conditions. Finally, the technique's high end-group fidelity at reasonably high conversion (80%) offers the opportunity for pre- and postfunctionalization, for example, with cell receptor specific targeting ligands and proteins.[58−60] Recently, we have reported on the RAFT copolymerization of (2,2-dimethyl-1,3-dioxolane-4-yl)methyl acrylate (DMDMA), a monomer containing a ketal functional group, with either methoxy tri(ethylene glycol) acrylate (mTEGA) or 2-hydroxyethyl acrylate (HEA).[61,62] These copolymers proved to exhibit LCST behavior, which can be tailored by varying the DMDMA feed ratio. The copolymers degraded into fully soluble unimers under acidic conditions and furthermore showed promising in vitro cytocompatibility. When using HEA as comonomer, a significantly faster degradation rate was witnessed. This can be ascribed to the higher exposure of the DMDMA units to the acidic aqueous medium in copolymers with HEA, whereas DMDMA units are more shielded from exposure to the aqueous environment in copolymers with the more bulky mTEGA monomer.

In this paper we report on the synthesis of responsive acid-degradable block copolymers based on HEA and DMDMA

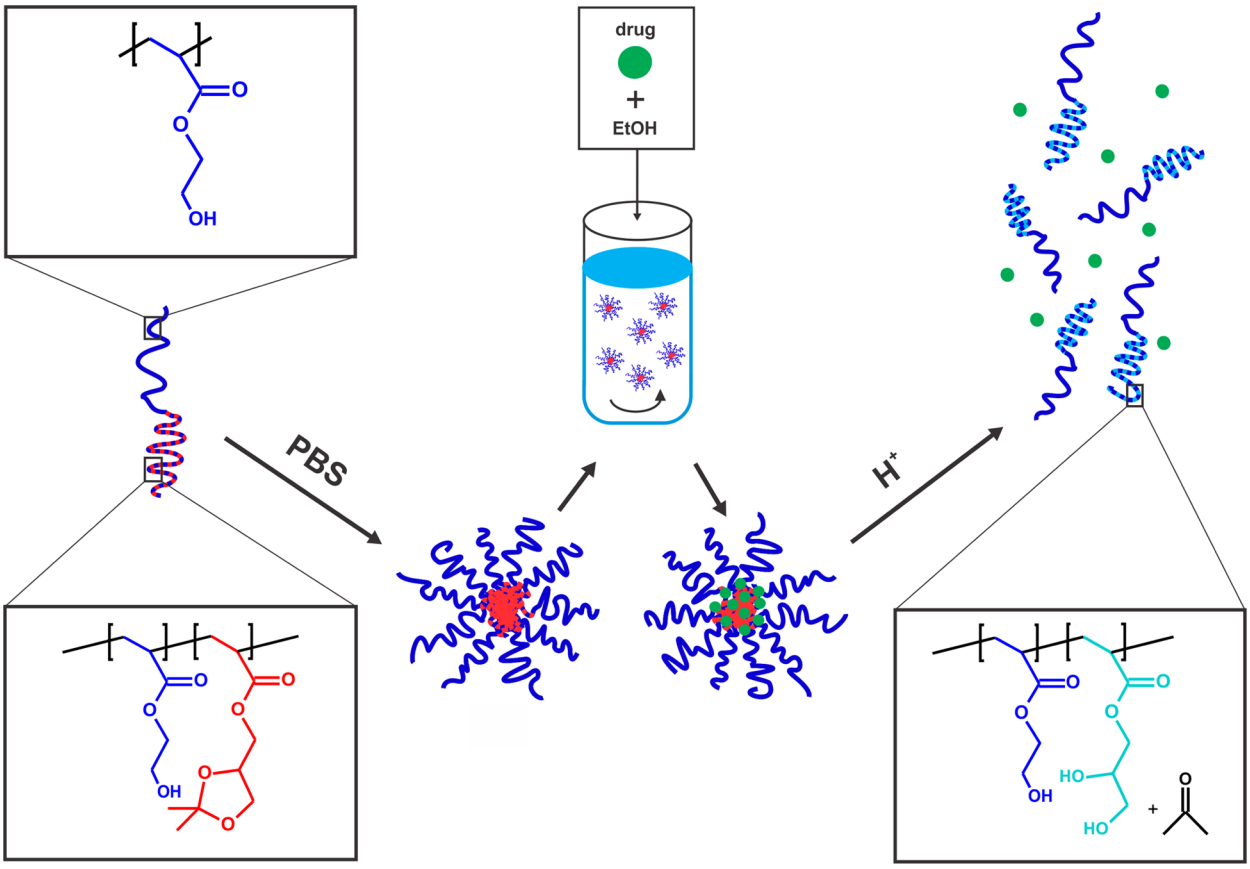

Figure 1. Self-assembly behavior, loading strategy (solvent displacement), and acid-triggered degradation of responsive poly(HEA)$_x$-*b*-poly(HEA$_m$-*co*-DMDMA$_n$)$_y$ block copolymer drug nanocarriers.

by RAFT polymerization, using a macroCTA (macro chain transfer agent) approach, to exploit the faster degradation of these copolymers.[63] The general block copolymer structure consists of a hydrophilic poly(HEA)$_x$ block and a (responsive) hydrophobic poly(HEA$_m$-*co*-DMDMA$_n$)$_y$ block, as shown in Figure 1. The main focus of this study was to systematically examine the influence of polymer design on self-assembly behavior, physicochemical properties (critical aggregation concentration (CAC), colloidal stability, and pH-responsive behavior), drug loading properties, and in vitro biological performance by varying the DMDMA content of the hydrophobic block. The applied loading strategy (solvent displacement) is shown in Figure 1, along with the rationale for acidic DMDMA hydrolysis. The latter involves the change of the hydrophobic ketal functional group into a hydrophilic glycerol moiety inducing supramolecular disassembly and release of payload, as the hydrophobic block gradually turns hydrophilic. In this way, we systematically evaluated the potential of these block copolymers for their use as nanocarrier for PTX as hydrophobic anticancer drug.

2. EXPERIMENTAL SECTION

2.1. Materials. All chemicals were purchased from Sigma-Aldrich unless mentioned otherwise. The RAFT agent 2-(butylthiocarbonothioylthio)propanoic acid (PABTC) and monomer (2,2-dimethyl-1,3-dioxolane-4-yl)methyl acrylate (DMDMA) were synthesized according to literature.[64,65] Octadecyl rhodamine B chloride (R18), enzyme-free cell dissociation buffer, Dulbecco's modified Eagle medium (DMEM), fetal bovine serum (FBS), L-glutamine, sodium pyruvate, penicillin, streptomycin, Hoechst, Alexa Fluor 647 Phalloidin, and LysoTracker Deep Red were obtained from Invitrogen. SKOV-3 cells were supplied by ATCC. Paclitaxel (PTX) was purchased from LC Laboratories.

2.2. Synthesis of Poly(HEA)$_x$ macroCTA. The macroCTA was synthesized by RAFT homopolymerization of 2-hydroxyethyl acrylate (HEA). PABTC (2 mmol, 0.476 g), 2,2′-azoisobutyronitrile (AIBN; 0.2 mmol, 0.033 g), and HEA (100 mmol, 11.612 g) were dissolved in *N*,*N*-dimethylformamide (DMF) to obtain a monomer concentration of 2 M and a monomer/CTA/initiator molar ratio of 50:1:0.1. The solution was bubbled with argon for 15 min. The reaction was performed at 70 °C under inert atmosphere, and the monomer conversion was monitored by gas chromatography (GC). The homopolymer was isolated by triple precipitation in cold (5 °C) diethyl ether and subsequently dried under high vacuum at room temperature. The homopolymer was analyzed by size exclusion chromatography (SEC).

GC samples were prepared by diluting 20 μL of polymerization mixture with 980 μL of methanol. GC was conducted on a 7890A system from Agilent Technologies equipped with an Agilent J&W Advanced Capillary GC column (30 m, 0.320 mm, and 0.25 μm). Injector and detector temperatures were kept constant at 250 and 280 °C, respectively. The column was initially set at 50 °C, followed by two heating stages: from 50 to 100 °C, with a rate of 20 °C/min, and from 100 to 300 °C, with a rate of 40 °C/min, and then held at this temperature for 0.5 min. Injections were performed with an Agilent Technologies 7693 auto sampler. Detection was done with a flame ionization detector. Conversion was determined based on the integration of monomer peaks using DMF as internal standard.

SEC was carried out on an Agilent 1260 system, equipped with a 1260 ISO-pump, a 1260 diode array detector (DAD), and a 1260 refractive index detector (RID). Measurements were performed in DMA containing 50 mM LiCl at 50 °C, using a flow rate of 0.593 mL/min. A guard column and two PL gel 5 μm mixed-D columns were used in series, calibrated with poly(methyl methacrylate) standards.

Scheme 1. Synthesis of (A) Poly(HEA)$_x$ MacroCTA and (B) Poly(HEA)$_x$-*b*-poly(HEA$_m$-*co*-DMDMA$_n$)$_y$[a]

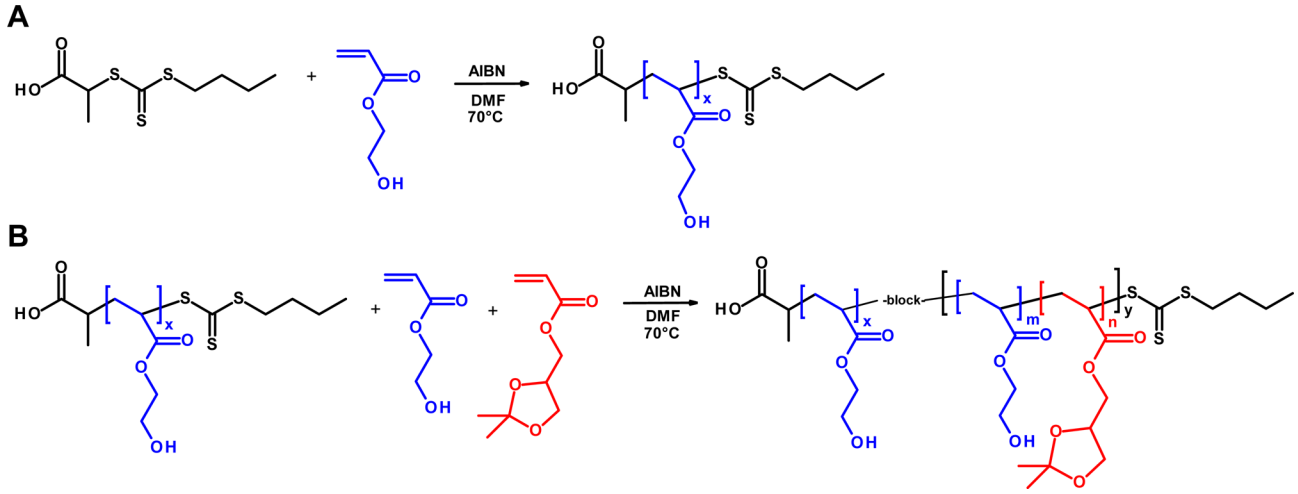

[a]HEA and DMDMA are depicted in blue and red, respectively.

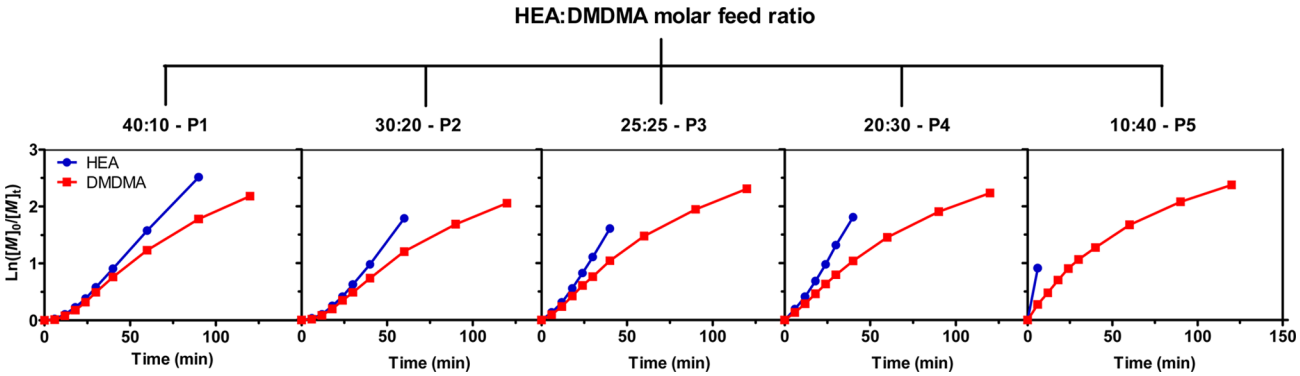

Figure 2. First order kinetic plots for the copolymerization of HEA (blue) and DMDMA (red) using the poly(HEA)$_x$ macroCTA resulting in poly(HEA)$_x$-*b*-poly(HEA$_m$-*co*-DMDMA$_n$)$_y$.

2.3. Synthesis and Characterization of Poly(HEA)$_x$-*b*-poly-(HEA$_m$-*co*-DMDMA$_n$)$_y$. The block copolymers were synthesized by RAFT copolymerization of HEA and DMDMA using the poly(HEA)$_x$ macroCTA described in section 2.2. A total of five block copolymers were synthesized for which the HEA/DMDMA molar feed ratio was 40:10, 30:20, 25:25, 20:30, and 10:40, respectively. All polymerizations were conducted within the same experimental setup using a Chemspeed ASW2000 automated synthesizer equipped with 16 parallel reactors of 13 mL, a Huber Petite Fleur thermostat for heating/cooling, a Huber Ministat 125 for reflux, and a Vacuubrand PC 3000 vacuum pump.[66]

Stock solutions (336.5 mg/mL macroCTA in DMF and 4.7 mg/mL AIBN in DMF) and monomers (HEA and DMDMA, neat) were bubbled with argon for 30 min before being introduced into the robot system and then kept under an argon atmosphere. The hood of the automated synthesizer was continuously flushed with nitrogen and the reactors were flushed with argon to ensure an inert atmosphere. Prior to the polymerizations, the reactors were deoxygenated through 10 vacuum−argon cycles. Stock solutions and monomers were transferred into the reactors using the liquid handling robot of the automated synthesizer. Each reactor eventually contained poly(HEA)$_x$ macroCTA (0.12 mmol, 0.514 g), AIBN (0.012 mmol, 2 mg), and 6 mmol of total monomer, dissolved in DMF to obtain a total monomer concentration of 1.8 M. The molar monomer$_{total}$/CTA/initiator ratio was 50:1:0.1. The reactions were run simultaneously at 70 °C. During the polymerizations, 50 μL samples were taken at preset time intervals for GC and SEC analysis. After the reactions, the block copolymers were purified by triple precipitation in cold diethyl ether and subsequent vacuum drying. Finally, all block copolymers were dialyzed (MWCO 3.5 kDa) for 4 days against water at 5 °C and recollected after freeze-drying.

The block copolymers were analyzed by SEC and ^{1}H NMR spectroscopy. ^{1}H NMR spectra were recorded on a Bruker 300 MHz FT-NMR spectrometer using chloroform-d or methanol-d$_4$ as solvent.

2.4. Self-Assembly and Temperature-Responsive Behavior in Aqueous Medium. Supramolecular and temperature-responsive self-assembly behavior in PBS was evaluated by dynamic light scattering (DLS). The block copolymers of poly(HEA)$_x$-*b*-poly(HEA$_m$-*co*-DMDMA$_n$)$_y$ (5 mg/mL) were sonicated for 15 min in cold (5 °C) PBS to induce faster dispersion compared to sonication at room temperature. After sonication, the samples were kept on ice overnight to allow complete dispersion. Next, the samples were filtered (0.450 μm) and measured at different temperatures (5, 20, and 37 °C). Measurements were carried out on a Zetasizer Nano S (Malvern).

2.5. Critical Aggregation Concentration (CAC). Similar to a described protocol, the CACs of poly(HEA)$_x$-*b*-poly(HEA$_m$-*co*-DMDMA$_n$)$_y$ were determined by fluorescence microscopy using pyrene as a fluorescent probe.[67,68] First, 2.5 mL polymer dispersions in PBS were made according to section 2.4 with concentrations ranging from 0.001 to 1 mg/mL. Second, a 3.6 mg/mL (1.8×10^{-2} M) stock solution of pyrene in acetone was prepared and kept on ice to prevent evaporation of the acetone. Next, 10 μL of this solution was diluted to 1 mL acetone and kept on ice. To each polymer dispersion, 8.3 μL of the latter pyrene solution was added under stirring leading to a pyrene concentration of 6.0×10^{-7} M. Fluorescence excitation spectra were collected at 20 °C on a Cary Eclipse fluorescence spectrophotometer (Agilent Technologies) equipped with a Varian Cary Temperature Controller. The CAC was quantified based on the

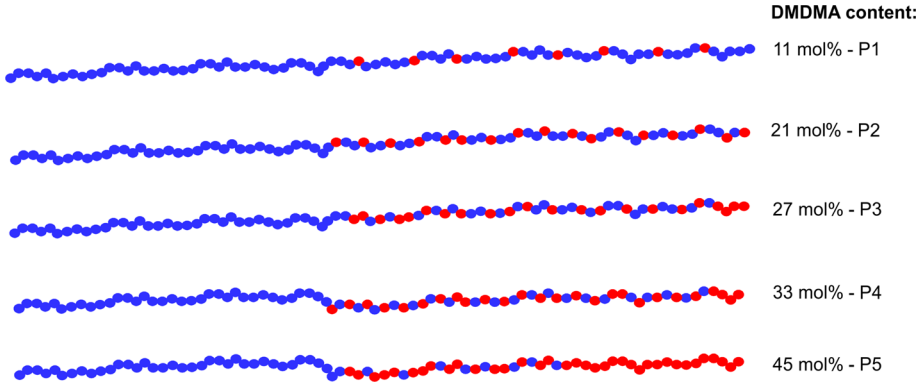

Figure 3. Average monomer distributions, calculated by regression analysis of the conversion vs time data, for the synthesized poly(HEA)$_x$-*b*-poly(HEA$_m$-*co*-DMDMA$_n$)$_y$ block copolymers. The blue and red dots represent HEA and DMDMA, respectively.

change in excitation intensity ratio at 338 and 333 nm with varying concentration.

2.6. In Vitro Stability and pH-responsive Behavior. Dispersions (5 mg/mL) of poly(HEA)$_x$-*b*-poly(HEA$_m$-*co*-DMDMA$_n$)$_y$ were prepared as described in section 2.4. DLS measurements were conducted over 4 days at 37 °C. On day 4, HCl was added under vigorous stirring to obtain a HCl concentration of 100 mM (pH 1). Subsequently, size and light scattering intensity was monitored by DLS. After 7 h incubation at 37 °C, a sample was taken from the acidic polymer dispersion and subsequently freeze-dried. The freeze-dried product was analyzed by ^{1}H NMR spectroscopy, using methanol-d_4 as solvent.

2.7. Cell Culture. SKOV-3 (human ovarian cancer cell line) cells were cultured in DMEM, supplemented with 10% FBS, 2 mM L-glutamine, 1 mM sodium pyruvate, and antibiotics (50 units/mL penicillin and 50 μg/mL streptomycin). Cells were incubated at 37 °C in a controlled, sterile environment of 95% relative humidity and 5% CO_2. SKOV-3 cells were used for all cell experiments.

2.8. In Vitro Cellular Uptake. *2.8.1. Encapsulation of Octadecyl Rhodamine B Chloride (R18).* A hydrophobic fluorescent dye (R18) was loaded into the nanoparticles using a solvent displacement technique. First, a 10 mg/mL stock solution of R18 in ethanol was prepared and kept on ice. Subsequently, 5 μL of this solution was diluted to 1 mL ethanol and kept on ice. Next, 1 mL of poly(HEA)$_x$-*b*-poly(HEA$_m$-*co*-DMDMA$_n$)$_y$ dispersions (10 mg/mL) were prepared in cold PBS according to section 2.4. Under stirring, 100 μL of the R18 working solution was added to 1 mL of block copolymer dispersion. Formulations were stabilized overnight at room temperature with an open lid to allow evaporation of the ethanol. Finally, excess dye was removed by membrane filtration (0.450 μm). Dilutions of 1 and 0.1 mg/mL block copolymer were prepared in PBS. In a similar way, a PBS control sample was prepared by adding 100 μL of R18 working solution to 1 mL of pure PBS under stirring, followed by overnight incubation at room temperature. Precipitated dye was removed by filtration.

2.8.2. Flow Cytometry (FACS). SKOV-3 cells were seeded into 24-well titer plates (250000 cells per well, suspended in 0.9 mL of culture medium) and incubated overnight to allow cell sedimentation and subsequent adhesion to the bottom of the wells. Next, 100 μL of R18-labeled poly(HEA)$_x$-*b*-poly(HEA$_m$-*co*-DMDMA$_n$)$_y$ (0.1, 1, or 10 mg/mL)/PBS control (section 2.8.1) was added to the cells (polymer concentration in well: 0.01, 0.1, or 1 mg/mL), followed by 24 h of incubation to allow cellular uptake. After incubation, the wells were aspirated and washed with 1 mL of PBS. After subsequent aspiration of the wells, 500 μL of cell dissociation buffer was added to the cells. The cells were completely detached from the wells after 15 min of incubation. The cell suspensions were transferred into Eppendorf tubes and immediately centrifuged (350 *g*, 15 min, 5 °C). Finally, the supernatant was aspirated and the cell pellets were suspended into 300 μL of PBS and kept on ice to maintain cell integrity.

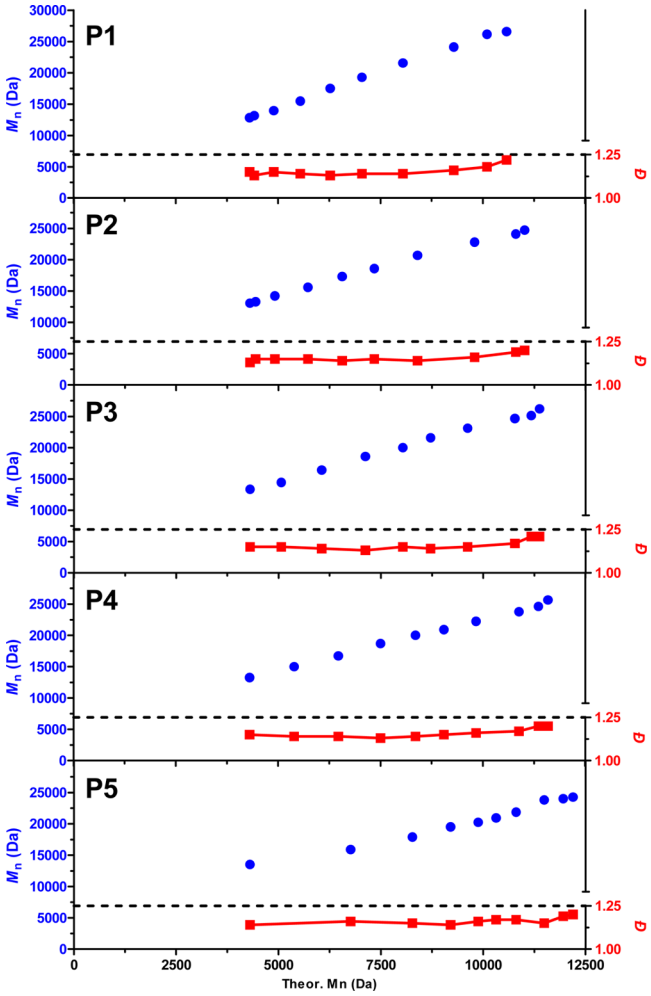

Figure 4. M_n and Đ (determined by SEC) plots as a function of theoretical M_n (based on GC) for the kinetic study for the synthesis of poly(HEA)$_x$-*b*-poly(HEA$_m$-*co*-DMDMA$_n$)$_y$.

FACS was performed on a BD Accuri C6 (BD Biosciences). The data were processed by FlowJo software.

2.8.3. Confocal Microscopy. First, a Hoechst stock solution of 1 mg/mL was prepared in dimethyl sulfoxide (DMSO). Alexa Fluor 647 Phalloidin was dissolved in 1.5 mL of methanol to obtain a stock concentration of 6.6 μM. Of these stock solutions, 6 and 35 μL were added, respectively, to 1.4 mL of PBS supplemented with 1% bovine serum albumin (BSA). The commercial LysoTracker Deep Red 1 mM stock solution was diluted in culture medium to a working

Table 2. Compositional Data for the Synthesized Polymers

polymer	$[HEA]_0/[CTA]$	conversion HEA[a] (%)	$[HEA]_0/[mCTA^e]$	conversion HEA[a] (%)	$[DMDMA]_0/[mCTA^e]$	conversion DMDMA[a] (%)	mol % DMDMA[b]	mol % DMDMA[c]	M_n[d] (kDa)	Đ[d]
	hydrophilic block		responsive block							
mCTA[e]	50	70							12.8	1.11
P1	50	70	40	100	10	89	11	12	26.6	1.22
P2	50	70	30	100	20	87	21	24	24.7	1.20
P3	50	70	25	100	25	90	27	27	26.2	1.21
P4	50	70	20	100	30	89	33	32	25.7	1.20
P5	50	70	10	100	40	91	45	39	24.3	1.20

[a]Calculated by GC using DMF as internal standard. [b]Overall DMDMA composition calculated by GC. [c]Overall DMDMA composition determined by ^{1}H NMR spectroscopy. [d]Analyzed by SEC. [e]mCTA = macroCTA.

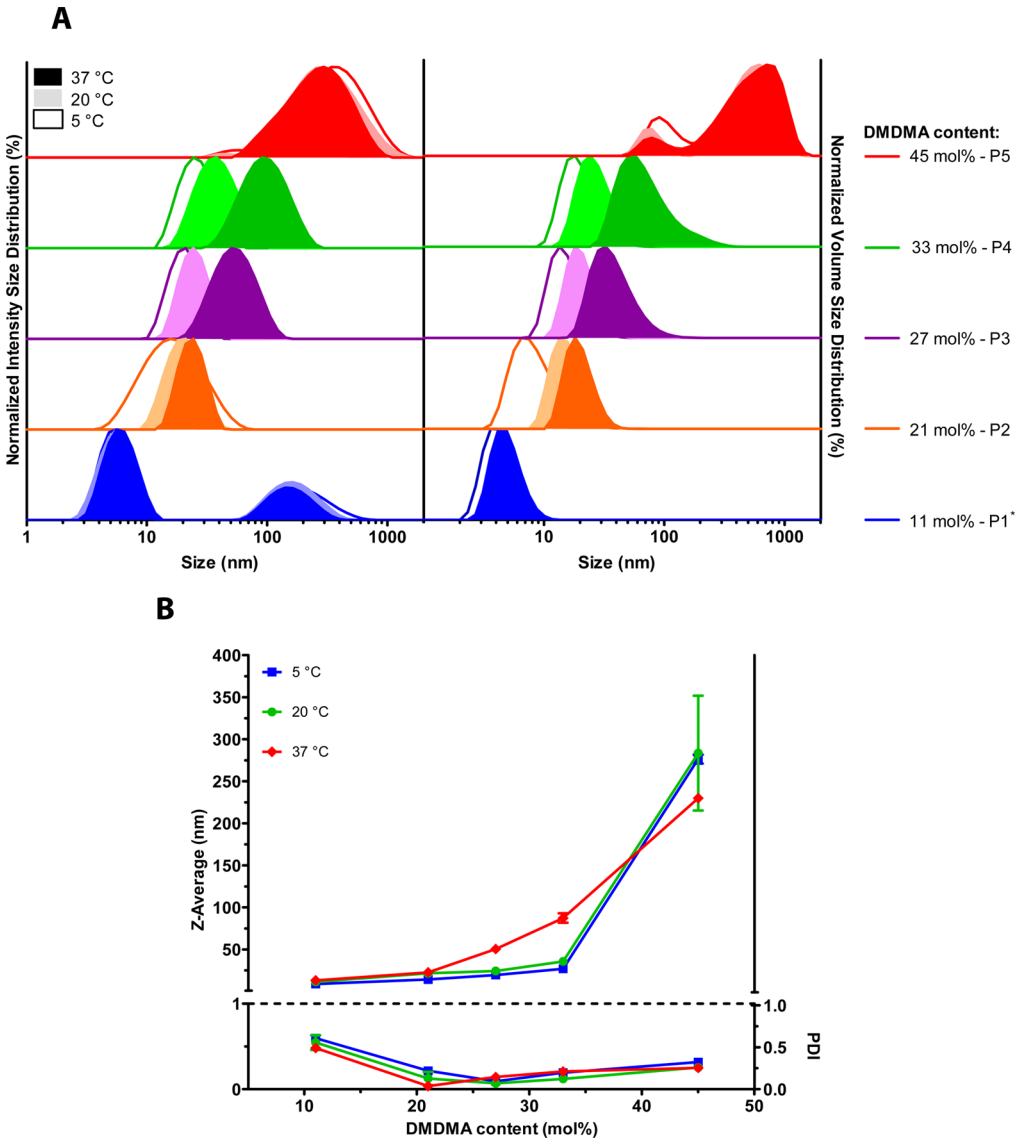

Figure 5. (A) Intensity size distribution histograms of poly(HEA)$_x$-*b*-poly(HEA$_m$-*co*-DMDMA$_n$)$_y$ (left panel), measured at different temperatures (5, 20, and 37 °C) by DLS. *The bimodal intensity size distribution of P1 shows a fraction of large particles. However, this fraction is very little and most likely associated with lose aggregates as it is not observed in the corresponding volume size distribution of the polymer (right panel). (B) *Z*-Average hydrodynamic diameter and PDI as a function of DMDMA content of poly(HEA)$_x$-*b*-poly(HEA$_m$-*co*-DMDMA$_n$)$_y$ (5 mg/mL), measured at 5, 20, and 37 °C by DLS (n = 3). Note that, due to the bimodal intensity size distribution and unimer state of P1, the corresponding values for *Z*-average hydrodynamic diameter and PDI are of little relevance.

concentration of 60 nM. SKOV-3 cells were plated out on Willco-Dish glass bottom dishes (50000 cells, suspended in 200 μL of culture medium) and incubated overnight. Next, 5 μL of 10 mg/mL R18-labeled poly(HEA)$_x$-*b*-poly(HEA$_m$-*co*-DMDMA$_n$)$_y$ (section 2.8.1) was added, followed by 24 h of incubation. R18 in pure PBS, described in section 2.8.1, was used as blank.

Simultaneous Hoechst and Alexa Fluor 647 Phalloidin staining was carried out on fixed cells. In summary, culture medium was aspirated

Table 3. Supramolecular Characteristics of Synthesized Block Copolymers

polymer	mol % DMDMA[a]	Z-avg[b] (nm) 5 °C	PDI[b] 20 °C	Z-avg[b] (nm) 37 °C	PDI[b]	Z-avg[b] (nm)	PDI[b]	CAC[c] (μg/mL)
P1	11	8.9 ± 0.4	0.61 ± 0.02	11.4 ± 1.8	0.56 ± 0.09	13.4 ± 1.0	0.49 ± 0.04	241 ± 15
P2	21	14.4 ± 0.1	0.22 ± 0.01	21.7 ± 3.4	0.13 ± 0.08	22.7 ± 0.2	0.04 ± 0.01	84 ± 4
P3	27	19.6 ± 0.6	0.10 ± 0.03	24.4 ± 1.2	0.07 ± 0.04	50.5 ± 1.8	0.15 ± 0.01	31 ± 1
P4	33	27.0 ± 0.8	0.20 ± 0.01	35.8 ± 5.0	0.12 ± 0.01	87.4 ± 5.6	0.21 ± 0.02	14 ± 1
P5	45	276.5 ± 5.3	0.32 ± 0.03	283.6 ± 68.2	0.26 ± 0.03	230.0 ± 3.7	0.25 ± 0.01	10 ± 1

[a]Overall DMDMA composition based on GC data. [b]Numeric values for Z-Average hydrodynamic diameter and PDI of poly(HEA)$_x$-*b*-poly-(HEA$_m$-*co*-DMDMA$_n$)$_y$, measured at 5, 20, and 37 °C (n = 3) by DLS. [c]CAC at 20 °C (n = 2).

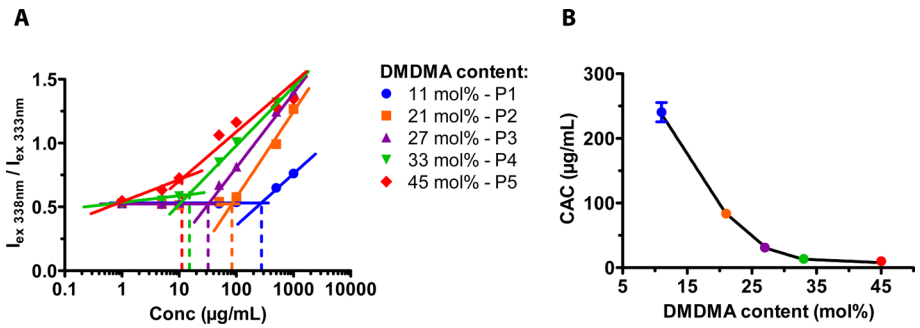

Figure 6. (A) Intensity ratio of pyrene at 338 nm (I_3) and 333 nm (I_1) as a function of poly(HEA)$_x$-*b*-poly(HEA$_m$-*co*-DMDMA$_n$)$_y$ concentration, determined by fluorescence spectrophotometry at 20 °C (n = 2). (B) CAC of poly(HEA)$_x$-*b*-poly(HEA$_m$-*co*-DMDMA$_n$)$_y$ at 20 °C as a function of DMDMA content (n = 2).

and cells were washed with PBS. Next, 200 μL of 4% paraformaldehyde was added and allowed to fixate for 15 min. After aspiration and washing, 200 μL of Hoechst-Alexa Fluor 647 Phalloidin working solution was added and incubated for 40 min at room temperature. Finally, the samples were washed with PBS.

Further, staining with LysoTracker Deep Red was performed on live cells. Briefly, culture medium was aspirated and cells were washed twice with PBS. Next, 200 μL of LysoTracker Deep Red working solution was added and allowed to incubate for 1.5 h before performing confocal microscopy. Confocal microscopy was carried out on a Leica DMI6000 B inverted microscope equipped with an oil immersion objective (Zeiss, 63×, NA 1.40) and attached to an Andor DSD2 confocal scanner. Images were processed with Imaris software.

2.9. Drug Loading. Paclitaxel (PTX) loaded poly(HEA)$_x$-*b*-poly(HEA$_m$-*co*-DMDMA$_n$)$_y$ nanoparticles were formulated based on the protocol described in section 2.8.1. A 5 mg/mL solution of PTX in ethanol was prepared and sealed to prevent solvent evaporation. Next, 1 mL of poly(HEA)$_x$-*b*-poly(HEA$_m$-*co*-DMDMA$_n$)$_y$ dispersions (10 mg/mL) were prepared in PBS, as described in section 2.4. To these polymer dispersions, 100 μL of PTX solution was added under vigorous stirring. The polymeric nanoparticles were allowed to stabilize overnight at room temperature, with the lid kept open to enable evaporation of the ethanol. Finally, precipitated PTX was removed by membrane filtration (0.450 μm).

To determine the concentration of loaded paclitaxel by LC-MS, the following sample preparation was performed. Briefly, 50 μL of PTX loaded nanoparticle dispersion was diluted into 950 μL of methanol. Of this solution 500 μL was 2-fold diluted in 500 μL of methanol. Finally, 100 μL of the latter dilution was added to 100 μL of Milli-Q water. Of the sample, 2 μL was injected into an Agilent 1200 series HPLC system equipped with a Phenomenex Luna C18 (2) (100 A, 50 × 2.00 mm, 3 μm) preceded by a Grace Alltima C18 (7.5 × 2.1 mm, 5 μm) guard column. The column temperature was 40 °C, and the sample compartment was maintained at room temperature. A binary solvent system was used in gradient mode with an initial flow rate of 0.2 mL/min. To allow shorter run times, this flow rate was increased to 0.3 mL/min after 5.6 min, maintained for 6 min, and then switched back to the initial flow rate to be maintained up to the end of the run (12.5 min). The solvents used were as follows: solvent A (90/10% v/v H2O/MeOH) and solvent B (100% v/v MeOH). The runs started with a 36/64 volume ratio of solvent A and B, which switched to 10/90 after 1.5 min. The latter ratio was maintained for 2.6 min and subsequently switched back to the initial ratio to be maintained up to the end of the run. The drug was detected by mass spectrometry using an API 3000 (AB Sciex) triple quadrupole mass spectrometer operated in the multiple reaction monitoring (MRM) mode. From the determined PTX concentration, encapsulation efficiency (EE) and loading capacity (LC) can be calculated. These parameters are defined by the formulas below:

$$\mathrm{EE} = \frac{\mathrm{concPTX(LC\text{-}MS)}}{\mathrm{concPTX(added)}} \times 100\%$$

$$\mathrm{LC} = \frac{\mathrm{concPTX(LC\text{-}MS)}}{\mathrm{concPTX(LC\text{-}MS)} + \mathrm{concpolymer(added)}} \times 100\%$$

2.10. In Vitro Cytotoxicity. The MTT assay was inspired on previously described methods in literature.[69,70] Dispersions of poly(HEA)$_x$-*b*-poly(HEA$_m$-*co*-DMDMA$_n$)$_y$ (10 mg/mL) were prepared in cold PBS as described in section 2.4. Of these dispersions, dilution series were made (concentrations ranging from 5 × 10^{-3} to 5 mg/mL). The PTX-loaded nanoparticles, prepared as described in section 2.9, were diluted (concentrations ranging from 5 × 10^{-5} to 50 μg/mL) along with two control nanoparticle formulations: Abraxane (Celgene) and Genexol-PM (Samyang Biopharmaceuticals). The MTT stock solution was prepared by dissolving 100 mg MTT in 20 mL of PBS and subsequent membrane filtration (0.220 μm). Before use, the MTT stock solution was 5-fold diluted with culture medium.

Briefly, SKOV-3 cells were seeded into 96-well titer plates (10000 cells per well, suspended in 200 μL of culture medium) and incubated overnight. Next, 50 μL of sample, DMSO (positive control = 0% viability) or PBS (negative control = 100% viability), was added to the cells, followed by 72 h of incubation. Subsequently, the medium was aspirated and the cells were washed with 250 μL of PBS. After aspiration, 100 μL of MTT working solution was added and the cells were incubated for 2.5 h. Finally, the MTT working solution was aspirated and the formed purple formazan crystals were dissolved in 50 μL of DMSO. Absorbance was determined at 590 nm using an EnVision Multilabel plate reader.

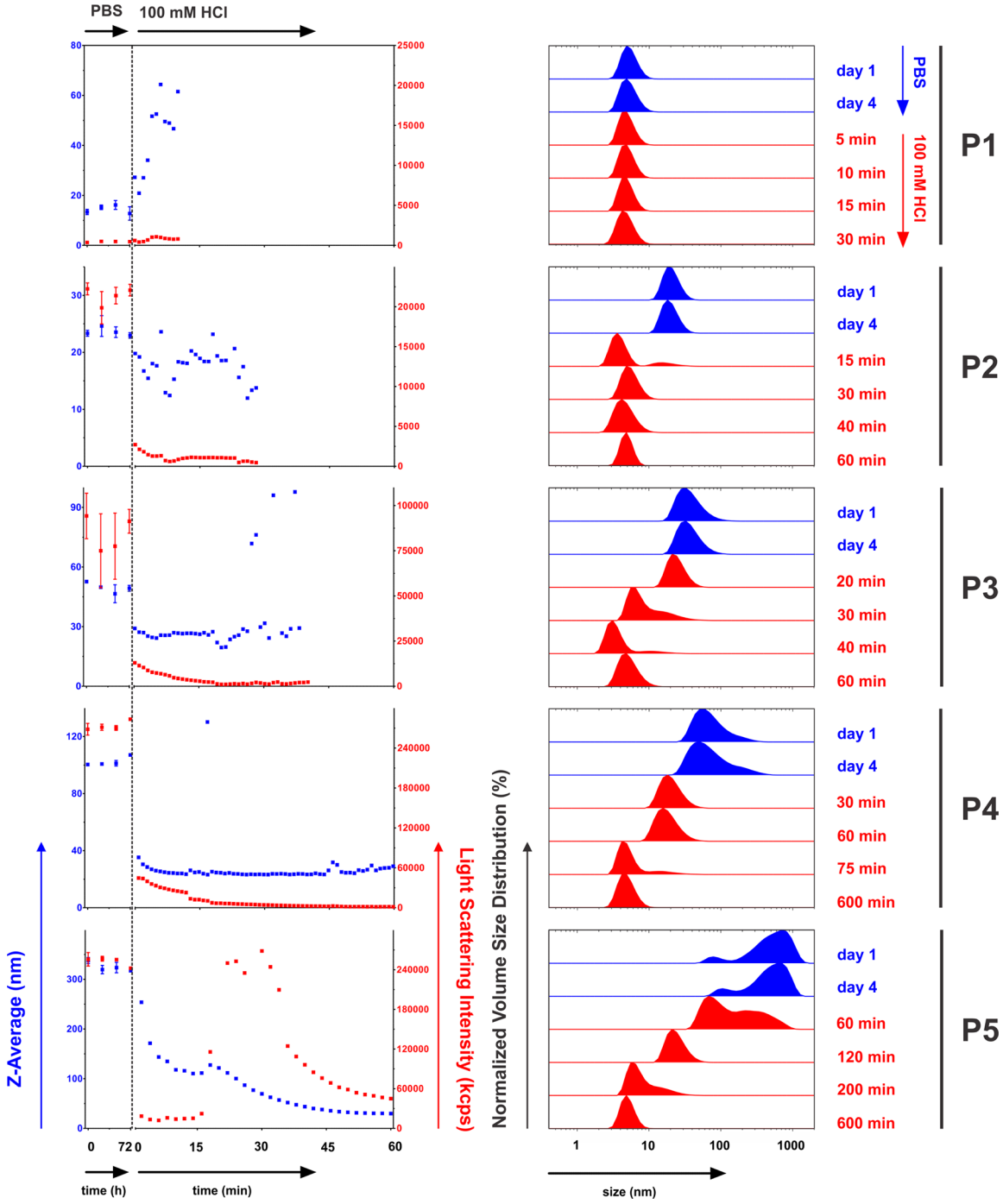

Figure 7. (Left panels) Z-Average diameter and light scattering intensity of the block copolymers as a function of time, measured at 37 °C by DLS. The block copolymers were measured over 4 days in PBS (n = 3), after which HCl was added to obtain a HCl concentration of 100 mM (pH 1). (Right panels) Corresponding volume distribution histograms.

The absorbance of the positive control was used as blank and therefore subtracted from all values. Cell viability (%) was defined as follows:

$$\text{cell viability} = \frac{\text{Abs(sample)} - \text{Abs(+control)}}{\text{Abs(−control)}} \times 100\%$$

3. RESULTS AND DISCUSSION

3.1. Synthesis of Poly(HEA)$_x$ MacroCTA. Amphiphilic block copolymers were prepared by sequential RAFT polymerization, starting with the synthesis of poly(2-hydroxyethyl acrylate) (poly(HEA)$_x$). This polymer serves as hydrophilic polymer block and is subsequently used as macroCTA for chain extension with a second responsive block consisting of both HEA as hydrophilic monomer and DMDMA as hydrophobic pH-degradable ketal monomer (Scheme 1A). Synthesis of poly(HEA)$_x$ was terminated at 70% conversion as determined by GC. SEC analysis in DMA showed a number-average molecular weight (M_n) of 12.8 kDa and a dispersity ($Đ$) of 1.11. No significant low or high molecular weight shoulders could be observed on the SEC trace (Figure S1), indicating the formation of a well-defined polymer. The latter is necessary for further use as macroCTA for subsequent block copolymerization.

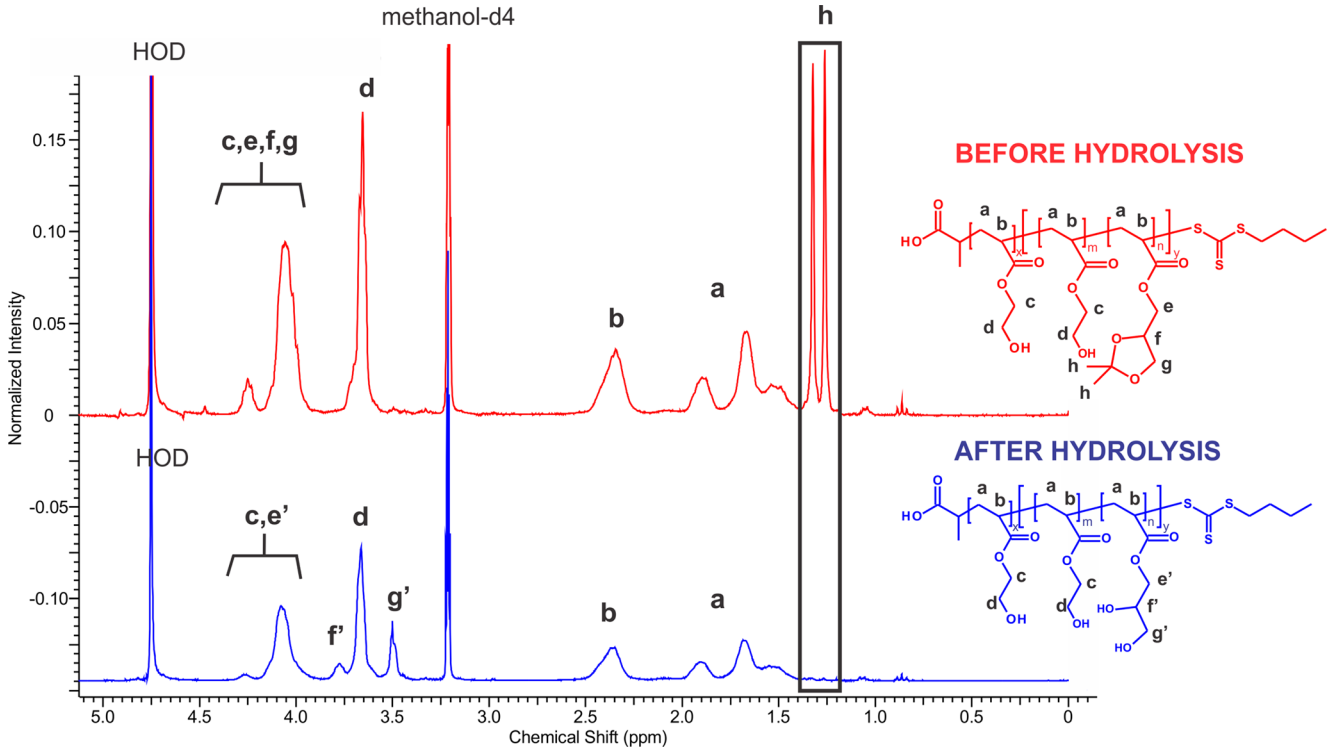

Figure 8. ^{1}H NMR spectrum of P2 (21 mol % DMDMA) before (red) and after (blue) hydrolysis. Note the absence of the ketal functional group after hydrolysis.

3.2. Synthesis and Characterization of Poly(HEA)$_x$-*b*-poly(HEA$_m$-*co*-DMDMA$_n$)$_y$. To allow for a systematic investigation on how the HEA:DMDMA feed ratio of the second block influences the structural block copolymer composition and properties, we used an automated synthesis robot. The advantage of this approach is, next to the obviously improved time efficiency, the reduced interexperiment variability as well as the ability to automatically withdraw samples during the polymerizations to study their kinetics. The poly(HEA)$_x$ macro-CTA was used as hydrophilic block to which five different HEA/DMDMA molar feed ratios (40:10, 30:20, 25:25, 20:30, 10:40) were added to form a hydrophobic, responsive second block (Scheme 1B). In addition to triple precipitation, the polymers were further purified by extensive dialysis to remove any residual solvent and monomer, as the latter two can influence in vitro cell culture experiments. Note that we did not synthesize block copolymers with a fully DMDMA-based hydrophobic block as preliminary experiments showed such block copolymers to form macroscopic aggregates in aqueous medium.

Kinetic samples of the copolymerization reactions were analyzed by GC and SEC (SEC traces are shown in Figure S2) to determine the evolution of monomer conversion and the resulting polymer molar mass (distribution) in time. Initially, a linear increase of $\mathrm{Ln}([M]_0/[M]_t)$ as a function of reaction time is observed for both HEA and DMDMA (Figure 2). After nearly complete consumption of HEA, the polymerization rate for DMDMA decreases indicating that the HEA chain end is more reactive toward DMDMA than the DMDMA chain end. The lower reactivity of DMDMA might be related to its bulkier side chain. The copolymerization behavior of HEA and DMDMA was also evaluated by determination of the reactivity ratios by nonlinear least-squares fitting of the incorporated HEA mole fraction (f_{HEA}) versus the theoretical HEA mole fraction (F_{HEA}) using the Contour software.[71] As the copolymerization with 10:40 HEA/DMDMA ratio was so fast that only one data point for HEA was obtained at $\mathrm{Ln}([M]_0/[M]_t)$ corresponding to 60% conversion, this copolymerization was not included in the fit. Furthermore, to exclude effects of equilibration of the RAFT polymerization process, f_{HEA} was determined at ∼30% conversion of HEA based on the GC kinetic data. The resulting reactivity ratios are $r_{\mathrm{HEA}} = 1.07 \pm 0.09$ and $r_{\mathrm{DMDMA}} = 0.62 \pm 0.07$, whereby it should be noted that these values are rough estimates as they are only based on four data points ($F_{\mathrm{HEA}} = 0.4$, 0.5, 0.6, and 0.8 with $f_{\mathrm{HEA}} = 0.472$, 0.557, 0.650, and 0.822, respectively). These reactivity ratios imply that the composition of the poly(HEA$_m$-*co*-DMDMA$_n$)$_y$ block gradually changes from being HEA rich to being DMDMA rich. This is schematically illustrated based on the calculated monomer distributions for the synthesized block copolymers by regression analysis of the GC kinetics (Figure 3). Furthermore, SEC analysis shows a linear increase of M_n with conversion and a narrow $Đ$ indicating good control over the polymerization (Figure 4). The composition of the different bock copolymers is listed in Table 2. For each block copolymer, a clear similarity is observed between the overall DMDMA composition when calculated from GC and ^{1}H NMR spectroscopy data. ^{1}H NMR spectra with peak integrations are shown in Figures S3−S7 for P1−P5.

3.3. Self-Assembly and Temperature-Responsive Behavior in Aqueous Medium. To investigate the influence of the DMDMA content on the self-assembly behavior and temperature-responsive properties, the block copolymers were dispersed (concentration 5 mg/mL) in cold phosphate buffered saline (PBS, pH 7.4, 150 mM NaCl) and subsequently measured by dynamic light scattering (DLS) at different temperatures (5, 20, and 37 °C). Normalized intensity and corresponding volume size distribution histograms of the particles, measured at increasing temperatures (5, 20, and 37 °C), are shown in Figure 5A. The corresponding *Z*-average hydrodynamic diameter and polydispersity

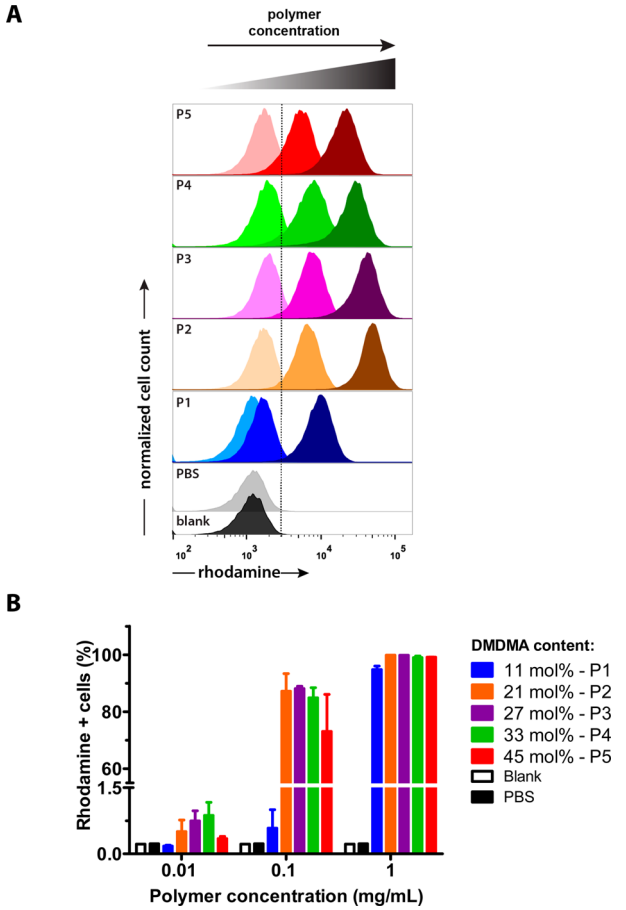

Figure 9. (A) Histograms of SKOV-3 cells, incubated for 24 h with 0.01, 0.1, and 1 mg/mL of R18-loaded poly(HEA)$_x$-*b*-poly(HEA$_m$-*co*-DMDMA$_n$)$_y$. (B) Corresponding percentage rhodamine + cells (n = 2).

(PDI) are plotted in Figure 5B as a function of temperature and the DMDMA content of the poly(HEA)$_x$-*b*-poly(HEA$_m$-*co*-DMDMA$_n$)$_y$ block copolymers (Table 2). A bimodal intensity size distribution is observed for the block copolymer with the lowest DMDMA content (i.e., 11 mol %, P1). The highest intensity is observed for a distribution with a size around 4 nm, representing soluble unimers. Furthermore, loose aggregates (60−300 nm) are detected, as often observed for thermoresponsive polymers.[72−74] However, the fraction of aggregates for P1 is limited, as the latter is not observed in the corresponding the volume size distribution of P1 (Figure 5A). The graphs show that the DMDMA content drastically affects the particle size. A larger particle diameter is measured with increasing DMDMA content. P2, P3, and P4 (containing 21, 27, and 33 mol % DMDMA, respectively) likely form micelles, whereas P5 (45 mol % DMDMA) forms larger assemblies. This trend is in line with the expectations as in aqueous medium, hydrophobic molecules are more likely to interact mutually than with water instead, therefore, generating larger assemblies.

The block copolymers with 21, 27, and 33 mol % DMDMA (P2, P3, and P4, respectively) show an increase in particle size upon increasing temperature, indicating the temperature-responsive behavior of these polymers. This influence of temperature was not unexpected, as our previously reported poly(mTEGA$_m$-*co*-DMDMA$_n$)$_y$ and poly(HEA$_m$-*co*-DMDMA$_n$)$_y$ copolymers exhibited similar LCST behavior.[61,62] On the other hand, temperature exerted minimal effect on the block copolymers

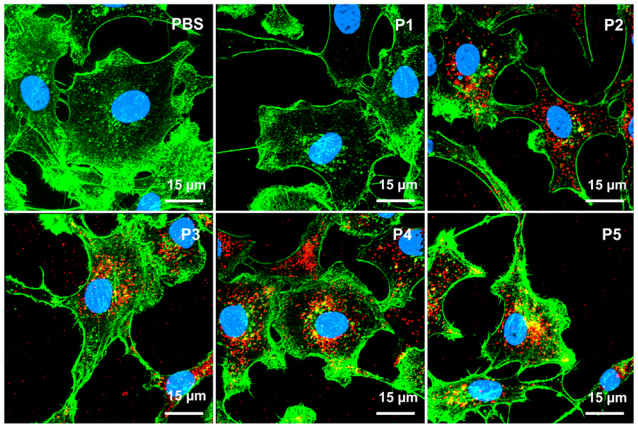

Figure 10. Maximized intensity projections (MIPs) of SKOV-3 cells, incubated for 24 h with R18-loaded poly(HEA)$_x$-*b*-poly(HEA$_m$-*co*-DMDMA$_n$)$_y$ (red). Cell nuclei and actin filaments are depicted in blue and green, respectively. Note that the Alexa Fluor 647 Phalloidin staining was performed without permeabilizing the cells to obtain a more selective staining of actin neighboring the cell membrane.

with the lowest (11 mol %, P1) and highest (45 mol %, P5) DMDMA content, which form either mainly soluble unimers (P1) or larger aggregates (P5), respectively, with constant size irrespective of temperature. Note that the observed trends in particle size are not due to time-dependent aggregation, as the nanoparticle size remained constant over at least 4 days, as shown further on in this paper (Figure 7). The values for *Z*-average hydrodynamic diameter and PDI against temperature are summarized for all block copolymers in Table 3. Note that a relatively low PDI is observed for all samples except for P1 due to its bimodal intensity size distribution.

3.4. Critical Aggregation Concentration (CAC). To compare the minimally required polymer concentration in aqueous medium for self-assembly of the different block copolymers, the excitation intensity ratio of pyrene at 338 nm (I_3) and 333 nm (I_1) was plotted versus the concentration of poly(HEA)$_x$-*b*-poly(HEA$_m$-*co*-DMDMA$_n$)$_y$ in PBS at 20 °C (Figure 6A). The subsequent calculated CACs are shown in Table 3 and Figure 6B (see Figure S8 for CAC fitting parameters of each block copolymer individually). The CAC of the block copolymers decreased from 241 to 10 μg/mL with increasing DMDMA content from 11 (P1) to 45 (P5) mol %. Increasing hydrophobicity contributes to lowering of CAC because of more pronounced hydrophobic interactions. The observation that P1 does show a relatively high CAC, although DLS does not show extensive particle formation (Figures 5A and 7), indicates that the presence of DMDMA does allow for a certain extent of hydrophobic interaction between pyrene and P1, possibly related to hydrophobic interactions occurring within the unimers or the loose aggregates. Similar observations were made by others, for example, Hennink and co-workers observed that addition of PTX from ethanol to an aqueous solution containing a temperature-responsive polymer below its phase transition temperature did not lead to immediate precipitation of PTX.[4] This behavior was ascribed to hydrophobic interaction between PTX and hydrophobic repeating units in the polymer backbone.

3.5. In Vitro Stability and pH-Responsive Behavior. At first, we aimed at investigating the colloidal stability of the block copolymer assemblies at pH 7.4 and gaining proof-of-concept for the acidic hydrolysis of the DMDMA repeating

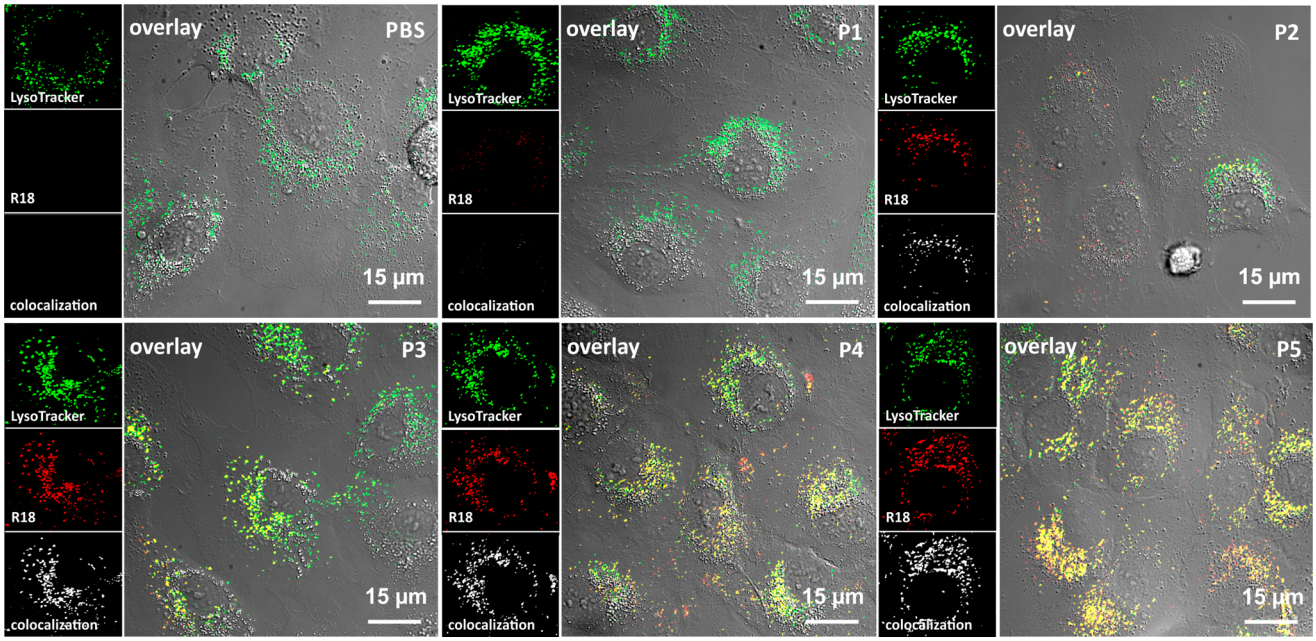

Figure 11. Confocal microscopy images of SKOV-3 cells, incubated for 24 h with R18-loaded poly(HEA)$_x$-*b*-poly(HEA$_m$-*co*-DMDMA$_n$)$_y$ (red). LysoTracker Deep Red was used for acidic organelle staining (green; note that this color was assigned for the sake of clarity and to allow rhodamine being assigned the red color). Colocalization of nanoparticles with these organelles (white) was analyzed using the colocalization function in the Imaris software package. Right panel: overlay of R18-loaded nanoparticles and acidic organelles with the corresponding differential interference contrast (DIC) image. The observed yellow color in the overlay panel also indicates colocalization.

units (Figure 1). To examine whether the poly(HEA)$_x$-*b*-poly(HEA$_m$-*co*-DMDMA$_n$)$_y$ nanoparticles are stable when dispersed in PBS or show aggregation over time, the block copolymer assemblies in PBS (see section 3.3) were measured over 4 days at 37 °C by DLS. Measurements were performed in triplicate. As shown in Figure 7, all nanoparticles remained stable at pH 7.4 for at least 4 days. Particle stability at physiological pH is essential to avoid premature drug release before the nanoparticles are internalized by cells.

On day 4, HCl was added to obtain a HCl concentration of 100 mM (pH 1). To examine the effect on the potential acidic hydrolysis of the ketal groups in the block copolymer side chains, the *Z*-average hydrodynamic diameter, light scattering intensity, and size volume distribution profiles were monitored by DLS. As shown in Figure 7, all block copolymer dispersions, except the block copolymer with 11 mol % DMDMA (P1), exhibit a gradual decrease in *Z*-average diameter, light scattering intensity, and volume size distribution. The reason that this is not observed for P1 can be ascribed to the unimer state of this polymer, which will not be affected by hydrolysis of its ketal moieties. The reason that often a bimodal distribution emerges during degradation is likely to be attributed to the inherent dynamic nature of block copolymer micelles, especially when their thermodynamic equilibrium is shifting due to hydrolysis of the DMDMA repeating units. The general decrease in size and scattering intensity suggest that in acidic medium, hydrolysis of the ketal groups effectively leads to decomposition of the block copolymer nanoparticles into soluble unimers. The latter is confirmed by ^{1}H NMR spectroscopy (Figure 8), showing complete absence of the ketal groups for the block copolymer with 21 mol % DMDMA (P2) after hydrolysis. Similar observations were done for the block copolymer with 45 mol % DMDMA (P5; Figure S9). Interestingly, from the evolution of the *Z*-average diameter and the scattering intensity as a function of time, one can observe that the rate of hydrolysis depends on the DMDMA content, with hydrolysis being significantly slower as the hydrophobic poly(HEA$_m$-*co*-DMDMA$_n$)$_y$ copolymer block contains more DMDMA repeating units and gradient structure. This slower hydrolysis can be ascribed to the stronger hydrophobic interactions within the polymers with higher DMDMA content, leading to stronger dehydration of the hydrophobic core domains and thereby decreased contact with HCl. Furthermore, a larger extent of DMDMA units needs to be hydrolyzed for the more hydrophobic block copolymers to render them hydrophilic enough for disassembly of the self-assembled structures.

3.6. In Vitro Cellular Uptake. Next, we investigated the potential of the block copolymers for intracellular delivery of a hydrophobic payload. For this purpose we used the SKOV-3 human ovarian cancer cell line. Block copolymer nanoparticles were loaded with octadecyl rhodamine B chloride (R18), a fluorescent dye suitable for staining embedded hydrophobic moieties (Figure S10).[75] The encapsulation was performed by adding a R18 stock solution in ethanol to a block copolymer dispersion (10 mg/mL) in PBS at a 1:10 volume ratio under stirring. R18 in pure PBS was used as a control. Subsequently, cellular uptake of the samples was assessed by flow cytometry (FACS) confocal microscopy.

Flow cytometry shows a dose-dependent increase in fluorescence (Figure 9A) and percentage of rhodamine positive cells (Figure 9B) for all poly(HEA)$_x$-*b*-poly(HEA$_m$-*co*-DMDMA$_n$)$_y$ nanoparticles, whereas no difference is observed between blank cells and cells pulsed with R18 in PBS. The latter indicates that the hydrophobic dye needs to be encapsulated in order to be internalized by cells. Earlier in this paper it was already shown that a 5 mg/mL dispersion in PBS of the block copolymer with 11 mol % DMDMA (P1) mainly consisted out of soluble unimers. This in turn explains why the R18-labeled formulation of P1 shows significantly lower cellular uptake compared to the other block copolymer formulations at the same concentration.

Confocal microscopy was used to investigate the intracellular fate of the block copolymer nanoparticles in more detail. In particular, confocal microscopy allows distinguishing between internalized and cell membrane bound nanoparticles. Fixed SKOV-3 cells were pulsed with Hoechst and Alexa Fluor 647 Phalloidin to stain the cell nuclei and the actin filaments, respectively. As shown in maximized intensity projections (MIPs; Figure 10), cellular uptake of R18-loaded particles (depicted in red) is observed for all block copolymers except P1. The latter was similar to the blank, which is in line with previous experiments showing absence of particle formation for this block copolymer. To further elucidate the intracellular fate of the observed nanoparticles, live SKOV-3 cells were stained with LysoTracker Deep Red. This is a fluorescent acidotropic probe, selectively accumulating in acidic organelles of live cells, for example, endosomes and lysosomes. Presence of fluorescent nanoparticles in these organelles is confirmed by colocalization between red and green fluorescence (Figure 11), suggesting active intracellular uptake of the nanoparticles.[76]

3.7. Drug Loading. To further explore the potential of the poly(HEA)$_x$-*b*-poly(HEA$_m$-*co*-DMDMA$_n$)$_y$ block copolymers for intracellular delivery of hydrophobic drugs, we used PTX as hydrophobic anticancer drug. Similar to R18 encapsulation, PTX-loading was performed by addition of a PTX solution in ethanol (5 mg/mL) to a block copolymer dispersion (10 mg/mL) with a 1:10 volume ratio. Unloaded drug can easily be eliminated by membrane filtration as PTX precipitates in aqueous medium due to its limited solubility (0.3 μg/mL).

The concentration of PTX in the samples after filtration was measured by LC-MS. As shown in Figure 12A, 4 out of 5 block copolymers solubilized significantly higher amounts of PTX than pure water. The block copolymer with 11 mol % DMDMA (P1) was not able to encapsulate PTX, fully in line with the observations of the previous DLS, CAC and FACS experiments. The almost identical structural composition of the block copolymers with 27 (P3) and 33 (P4) mol % DMDMA (Figure 3) probably results in comparable interaction with PTX and therefore similar PTX solubility. Nanoparticles of the block copolymer with 45 mol % DMDMA (P5) did not encapsulate higher concentrations of PTX compared to block copolymers with 27 (P3) or 33 (P4) mol % DMDMA. This can be explained based on the size distribution histograms of the block copolymer at 20 °C (Figure 5A). This shows that a significant amount of particles is larger than 450 nm, which could have been removed during membrane filtration (0.450 μm). A similar trend is observed in Figure 12B for the calculated encapsulation efficiencies (EE) and loading capacities (LC), earlier defined in section 2.9. DLS analysis of the PTX-loaded block copolymer nanoparticles showed no significant change in size compared to empty nanoparticles (data not shown).

3.8. In Vitro Cytotoxicity. The in vitro cytotoxicity of empty and paclitaxel loaded poly(HEA)$_x$-*b*-poly(HEA$_m$-*co*-DMDMA$_n$)$_y$ nanoparticles was evaluated on SKOV-3 cells via MTT assay. Abraxane and Genexol-PM were included for comparison. Abraxane is a formulation of albumin stabilized PTX nanocrystals, while Genexol-PM consists of PTX-loaded polymeric micelles based on monomethoxy poly(ethylene glycol)-*block*-poly(D,L-lactide) (mPEG-*b*-PDLLA).[77] An incubation period of 72 h was used to evaluate the known inhibitory effect of PTX on (cancer) cell proliferation. According to ISO 10993−5, cell viability below 70% in comparison to negative control indicates cytotoxicity.

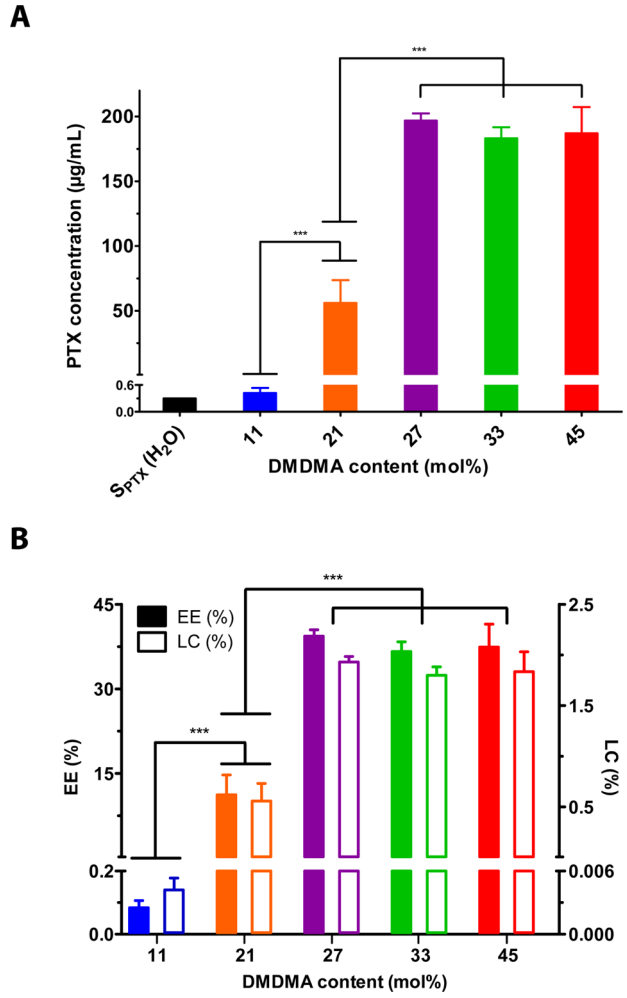

Figure 12. (A) Concentration of PTX, encapsulated by poly(HEA)$_x$-*b*-poly(HEA$_m$-*co*-DMDMA$_n$)$_y$, measured by LC-MS (n = 5). (B) Calculated encapsulation efficiency (EE) and loading capacity (LC) of PTX-loaded poly(HEA)$_x$-*b*-poly(HEA$_m$-*co*-DMDMA$_n$)$_y$. ***Student's *t*-test: $p < 0.001$.

As shown in Figure 13A, no significant intrinsic cytotoxic effect can be ascribed to any of the block copolymers at concentrations up to 1 mg/mL. The formation of acetone (Figure 1) upon hydrolysis of the ketal moieties does not seem to affect the cell viability. This suggests that the synthesized block copolymers are cytocompatible, at least within the presently applied experimental setting. Significant in vitro cytotoxicity was observed for block copolymer formulations with PTX concentrations ranging from 0.01 to 10 μg/mL (Figure 13B). The cytotoxic effect was comparable or, in the case of PTX concentrations of 0.1 and 0.01 μg/mL, more potent than Abraxane and Genexol-PM. Based on the determined CACs, the PTX formulations prepared from the block polymers with a DMDMA content >11 mol % (section 2.9) were below their CAC at a PTX concentration of 0.1 μg/mL. The formulation prepared from the 11 mol % DMDMA block copolymer (P1) was below CAC at a PTX concentration of 0.01 μg/mL. Note that for the latter formulation, PTX concentrations of 10 and 1 μg/mL could not be obtained. Taking CAC into account, along with the in vitro stability of the nanoparticles (section 3.5), the cytotoxic effect will likely be due to a combination of PTX that is efficiently solubilized in culture medium and PTX that is released after endocytosis by degradation of the DMDMA units.

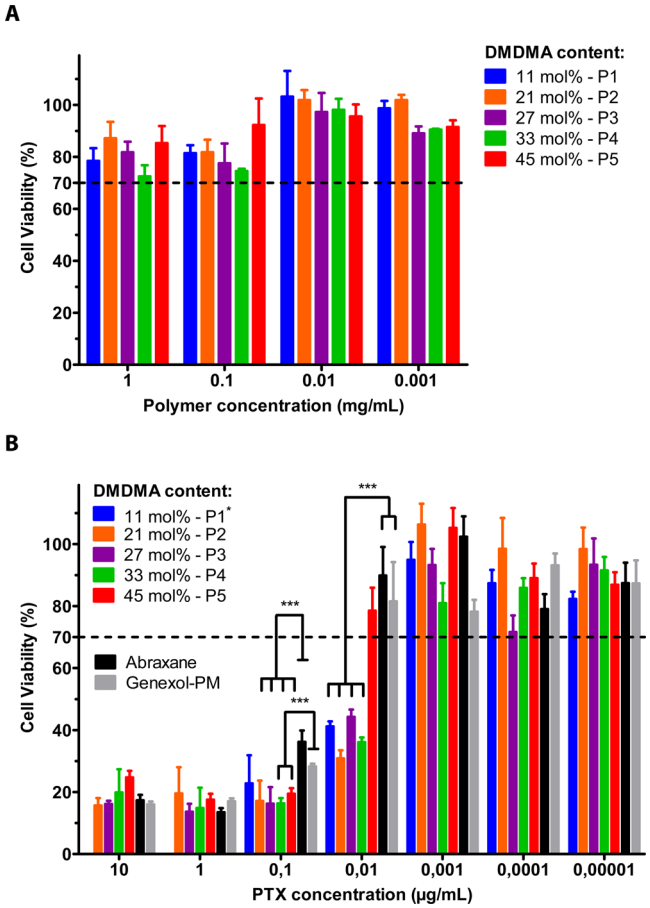

Figure 13. (A) In vitro cytotoxicity of unloaded poly(HEA)$_x$-*b*-poly(HEA$_m$-*co*-DMDMA$_n$)$_y$ on SKOV-3 cells after 72 h of incubation (n = 3). (B) In vitro cytotoxicity of PTX-loaded poly(HEA)$_x$-*b*-poly(HEA$_m$-*co*-DMDMA$_n$)$_y$ on SKOV-3 cells after 72 h of incubation (n = 3). Abraxane and Genexol-PM were used as control. *PTX well concentrations of 10 and 1 μg/mL could not be obtained for P1. ***Student's t-test: $p < 0.001$.

Future research will aim at elucidating the pH-induced release of the drug inside the complex intracellular medium and its relative contribution on PTX-induced cytotoxicity.

4. CONCLUSION

Well-defined responsive poly(HEA)$_x$-*b*-poly(HEA$_m$-*co*-DMDMA$_n$)$_y$ block copolymers were synthesized with good control by sequential RAFT polymerization. Kinetic studies revealed that the reactivity ratios for the HEA:DMDMA copolymerization of the second block are r_{HEA} = 1.07 ± 0.09 and r_{DMDMA} = 0.62 ± 0.07. We have shown that the DMDMA content strongly influences aqueous self-assembly behavior, CAC and stimuli-responsive properties. A content of >11 mol % DMDMA is required to afford the formation of nanoparticles in aqueous medium. All particles proved to be stable in PBS at 37 °C for at least 4 days and turned fully water-soluble upon acid-triggered hydrolysis. This should allow the polymers to be cleared from the body by renal filtration. Active cellular uptake was observed in vitro by flow cytometry and confocal microscopy. PTX could be loaded into the nanoparticles by solvent displacement, increasing PTX solubility in water by a factor of up to 650. Of these formulations, in vitro cytotoxicity comparable or better than two commercial PTX nanoformulations was observed, while empty particles did not induce any significant cytotoxic effect.

Due to these promising preliminary in vitro results, our current investigations aim at further exploring ketal-based systems for the design of anticancer drug nanocarriers that could, owing to their small size (i.e., the most promising systems in this paper had a Z-average hydrodynamic diameter around 20, 50, and 100 nm, respectively), penetrate deep into poorly vascularized metastatic tumor tissue. We will, for example, consider cross-linking strategies to further lower the CAC. Additionally, we aim in the future at engineering the nanoparticle surface with ligands that afford active targeting of receptors that are overexpressed by ovarian cancer cells, such as the folate receptor alpha (FR$_\alpha$) and CD44 receptor.[78−81]

■ ASSOCIATED CONTENT

Supporting Information

Additional data/information includes (kinetic) SEC-traces of macroCTA and block copolymers, ^{1}H NMR spectra and CAC fitting parameters of P1 → P5, ^{1}H NMR spectrum of hydrolyzed P5, and molecular structure of octadecyl rhodamine B chloride. This material is available free of charge via the Internet at http://pubs.acs.org.

■ AUTHOR INFORMATION

Corresponding Authors

*E-mail: br.degeest@ugent.be.
*E-mail: richard.hoogenboom@ugent.be.

Notes

The authors declare no competing financial interest.

■ ACKNOWLEDGMENTS

B.L. thanks the Agency for Innovation by Science and Technology in Flanders (IWT) for Ph.D. scholarship. B.G.D.G. and R.H. acknowledge Ghent University (BOF) and FWO-Flanders for funding. Q.Z. and N.V. wish to thank Ghent University (BOF) for Ph.D. scholarships. Q.Z. and Y.S. thank the China Scholarship Council (CSC) for granting Ph.D. scholarships.

■ REFERENCES

(1) Baguley, B. C.; Kerr, D. J. *Anticancer Drug Development.*, 1st ed.; Academic Press: San Diego, 2001; p 397.
(2) Panchagnula, R. Pharmaceutical Aspects of Paclitaxel. *Int. J. Pharm.* **1998**, *172* (1−2), 1−15.
(3) Lee, S. C.; Huh, K. M.; Lee, J.; Cho, Y. W.; Galinsky, R. E.; Park, K. Hydrotropic Polymeric Micelles for Enhanced Paclitaxel Solubility: In Vitro and In Vivo Characterization. *Biomacromolecules* **2007**, *8* (1), 202−208.
(4) Soga, O.; van Nostrum, C. F.; Fens, M.; Rijcken, C. J. F.; Schiffelers, R. M.; Storm, G.; Hennink, W. E. Thermosensitive and Biodegradable Polymeric Micelles for Paclitaxel Delivery. *J. Controlled Release* **2005**, *103* (2), 341−353.
(5) Lee, H.; Lee, K.; Park, T. G. Hyaluronic Acid-Paclitaxel Conjugate Micelles: Synthesis, Characterization, and Antitumor Activity. *Bioconjugate Chem.* **2008**, *19* (6), 1319−1325.
(6) Gelderblom, H.; Verweij, J.; Nooter, K.; Sparreboom, A. Cremophor EL: The Drawbacks and Advantages of Vehicle Selection for Drug Formulation. *Eur. J. Cancer* **2001**, *37* (13), 1590−1598.
(7) Rivkin, I.; Cohen, K.; Koffler, J.; Melikhov, D.; Peer, D.; Margalit, R. Paclitaxel-Clusters Coated with Hyaluronan as Selective Tumor-Targeted Nanovectors. *Biomaterials* **2010**, *31* (27), 7106−7114.

(8) Chen, H. B.; Khemtong, C.; Yang, X. L.; Chang, X. L.; Gao, J. M. Nanonization Strategies for Poorly Water-Soluble Drugs. *Drug Discovery Today* **2011**, *16* (7−8), 354−360.
(9) Johnston, A. P. R.; Such, G. K.; Ng, S. L.; Caruso, F. Challenges Facing Colloidal Delivery Systems: From Synthesis to the Clinic. *Curr. Opin. Colloid Interface Sci.* **2011**, *16* (3), 171−181.
(10) Venditto, V. J.; Szoka, F. C. Cancer Nanomedicines: So Many Papers and so Few Drugs! *Adv. Drug Delivery Rev.* **2013**, *65* (1), 80−88.
(11) Davis, M. E.; Chen, Z.; Shin, D. M. Nanoparticle Therapeutics: An Emerging Treatment Modality for Cancer. *Nat. Rev. Drug Discovery* **2008**, *7* (9), 771−782.
(12) Peer, D.; Karp, J. M.; Hong, S.; FaroKhzad, O. C.; Margalit, R.; Langer, R. Nanocarriers as an Emerging Platform for Cancer Therapy. *Nat. Nanotechnol.* **2007**, *2* (12), 751−760.
(13) Duncan, R. Polymer Conjugates As Anticancer Nanomedicines. *Nat. Rev. Cancer* **2006**, *6* (9), 688−701.
(14) Maeda, H.; Wu, J.; Sawa, T.; Matsumura, Y.; Hori, K. Tumor Vascular Permeability and the EPR Effect in Macromolecular Therapeutics: A Review. *J. Controlled Release* **2000**, *65* (1−2), 271−284.
(15) Wang, A. Z.; Langer, R.; Farokhzad, O. C. Nanoparticle Delivery of Cancer Drugs. *Annu. Rev. Med.* **2012**, *63*, 185−198.
(16) Miele, E.; Spinelli, G. P.; Tomao, F.; Tomao, S. Albumin-Bound Formulation of Paclitaxel (Abraxane (R) ABI-007) in the Treatment of Breast Cancer. *Int. J. Nanomed.* **2009**, *4* (1), 99−105.
(17) Ma, J. K. C.; Drake, P. M. W.; Christou, P. The Production of Recombinant Pharmaceutical Proteins in Plants. *Nat. Rev. Genet.* **2003**, *4* (10), 794−805.
(18) Kamaly, N.; Xiao, Z. Y.; Valencia, P. M.; Radovic-Moreno, A. F.; Farokhzad, O. C. Targeted Polymeric Therapeutic Nanoparticles: Design, Development and Clinical Translation. *Chem. Soc. Rev.* **2012**, *41* (7), 2971−3010.
(19) Upadhyay, K. K.; Le Meins, J. F.; Misra, A.; Voisin, P.; Bouchaud, V.; Ibarboure, E.; Schatz, C.; Lecommandoux, S. Biomimetic Doxorubicin Loaded Polymersomes from Hyaluronan-*block*-Poly(γ-benzyl glutamate) Copolymers. *Biomacromolecules* **2009**, *10* (10), 2802−2808.
(20) Lee, E. S.; Na, K.; Bae, Y. H. Polymeric Micelle for Tumor pH and Folate-Mediated Targeting. *J. Controlled Release* **2003**, *91* (1−2), 103−113.
(21) Zhao, X. Y.; Poon, Z.; Engler, A. C.; Bonner, D. K.; Hammond, P. T. Enhanced Stability of Polymeric Micelles Based on Postfunctionalized Poly(ethylene glycol)-*b*-Poly(γ-propargyl L-glutamate): The Substituent Effect. *Biomacromolecules* **2012**, *13* (5), 1315−1322.
(22) Shi, Y.; van den Dungen, E. T. A.; Klumperman, B.; van Nostrum, C. F.; Hennink, W. E. Reversible Addition-Fragmentation Chain Transfer Synthesis of a Micelle-Forming, Structure Reversible Thermosensitive Diblock Copolymer Based on the *N*-(2-Hydroxy propyl) Methacrylamide Backbone. *ACS Macro Lett.* **2013**, *2* (5), 403−408.
(23) Smith, A. E.; Xu, X. W.; McCormick, C. L. Stimuli-Responsive Amphiphilic (Co)Polymers via RAFT Polymerization. *Prog. Polym. Sci.* **2010**, *35* (1−2), 45−93.
(24) Huang, X.; Appelhans, D.; Formanek, P.; Simon, F.; Voit, B. Tailored Synthesis of Intelligent Polymer Nanocapsules: An Investigation of Controlled Permeability and pH-Dependent Degradability. *ACS Nano* **2012**, *6* (11), 9718−9726.
(25) Smart, T.; Lomas, H.; Massignani, M.; Flores-Merino, M. V.; Perez, L. R.; Battaglia, G. Block Copolymer Nanostructures. *Nano Today* **2008**, *3* (3−4), 38−46.
(26) Venkataraman, S.; Hedrick, J. L.; Ong, Z. Y.; Yang, C.; Ee, P. L. R.; Hammond, P. T.; Yang, Y. Y. The Effects of Polymeric Nanostructure Shape on Drug Delivery. *Adv. Drug Delivery Rev.* **2011**, *63* (14−15), 1228−1246.
(27) Schroeder, A.; Heller, D. A.; Winslow, M. M.; Dahlman, J. E.; Pratt, G. W.; Langer, R.; Jacks, T.; Anderson, D. G. Treating Metastatic Cancer with Nanotechnology. *Nat. Rev. Cancer* **2012**, *12* (1), 39−50.
(28) Bae, Y.; Jang, W. D.; Nishiyama, N.; Fukushima, S.; Kataoka, K. Multifunctional Polymeric Micelles with Folate-Mediated Cancer Cell Targeting and pH-Triggered Drug Releasing Properties for Active Intracellular Drug Delivery. *Mol. BioSyst.* **2005**, *1* (3), 242−250.
(29) Yokoyama, M. Polymeric Micelles As a New Drug Carrier System and Their Required Considerations for Clinical Trials. *Expert Opin. Drug Delivery* **2010**, *7* (2), 145−158.
(30) Kim, S.; Shi, Y. Z.; Kim, J. Y.; Park, K.; Cheng, J. X. Overcoming the Barriers in Micellar Drug Delivery: Loading Efficiency, In Vivo Stability, and Micelle−Cell Interaction. *Expert Opin. Drug Delivery* **2010**, *7* (1), 49−62.
(31) Gong, J.; Chen, M. W.; Zheng, Y.; Wang, S. P.; Wang, Y. T. Polymeric Micelles Drug Delivery System in Oncology. *J. Controlled Release* **2012**, *159* (3), 312−323.
(32) Deng, C.; Jiang, Y. J.; Cheng, R.; Meng, F. H.; Zhong, Z. Y. Biodegradable Polymeric Micelles for Targeted and Controlled Anticancer Drug Delivery: Promises, Progress and Prospects. *Nano Today* **2012**, *7* (5), 467−480.
(33) Bourzac, K. Nanotechnology Carrying Drugs. *Nature* **2012**, *491* (7425), S58−S60.
(34) Fleige, E.; Quadir, M. A.; Haag, R. Stimuli-Responsive Polymeric Nanocarriers for the Controlled Transport of Active Compounds: Concepts and Applications. *Adv. Drug Delivery Rev.* **2012**, *64* (9), 866−884.
(35) Pietsch, C.; Mansfeld, U.; Guerrero-Sanchez, C.; Hoeppener, S.; Vollrath, A.; Wagner, M.; Hoogenboom, R.; Saubern, S.; Thang, S. H.; Becer, C. R.; Chiefari, J.; Schubert, U. S. Thermo-Induced Self-Assembly of Responsive Poly(DMAEMA-*b*-DEGMA) Block Copolymers into Multi- and Unilamellar Vesicles. *Macromolecules* **2012**, *45* (23), 9292−9302.
(36) Quadir, M. A.; Morton, S. W.; Deng, Z. J.; Shopsowitz, K. E.; Murphy, R. P.; Epps, T. H.; Hammond, P. T. PEG-Polypeptide Block Copolymers as pH-Responsive Endosome-Solubilizing Drug Nanocarriers. *Mol. Pharmaceutics* **2014**, *11* (7), 2420−2430.
(37) Randolph, L. M.; Chien, M. P.; Gianneschi, N. C. Biological Stimuli and Biomolecules in the Assembly and Manipulation of Nanoscale Polymeric Particles. *Chem. Sci.* **2012**, *3* (5), 1363−1380.
(38) FitzGerald, P. A.; Gupta, S.; Wood, K.; Perrier, S.; Warr, G. G. Temperature- and pH-Responsive Micelles with Collapsible Poly(*N*-isopropylacrylamide) Headgroups. *Langmuir* **2014**, *30* (27), 7986−7992.
(39) Yao, Z. L.; Tam, K. C. Temperature Induced Micellization and Aggregation of Biocompatible Poly(oligo(ethylene glycol)methyl ether methacrylate) Block Copolymer Analogs in Aqueous Solutions. *Polymer* **2012**, *53* (16), 3446−3453.
(40) Hoogenboom, R. Poly(2-oxazoline)s: A Polymer Class with Numerous Potential Applications. *Angew. Chem., Int. Ed.* **2009**, *48* (43), 7978−7994.
(41) Vancoillie, G.; Frank, D.; Hoogenboom, R. Thermoresponsive Poly(oligo ethylene glycol acrylates). *Prog. Polym. Sci.* **2014**, *39* (6), 1074−1095.
(42) Du, J. Z.; Tang, Y. Q.; Lewis, A. L.; Armes, S. P. pH-Sensitive Vesicles Based on a Biocompatible Zwitterionic Diblock Copolymer. *J. Am. Chem. Soc.* **2005**, *127* (51), 17982−17983.
(43) Heller, J.; Barr, J.; Ng, S. Y.; Shen, H. R.; Schwach-Abdellaoui, K.; Emmahl, S.; Rothen-Weinhold, A.; Gurny, R. Poly(ortho esters) - Their Development and Some Recent Applications. *Eur. J. Pharm. Biopharm.* **2000**, *50* (1), 121−128.
(44) Shenoi, R. A.; Narayanannair, J. K.; Hamilton, J. L.; Lai, B. F. L.; Horte, S.; Kainthan, R. K.; Varghese, J. P.; Rajeev, K. G.; Manoharan, M.; Kizhakkedathu, J. N. Branched Multifunctional Polyether Polyketals: Variation of Ketal Group Structure Enables Unprecedented Control over Polymer Degradation in Solution and within Cells. *J. Am. Chem. Soc.* **2012**, *134* (36), 14945−14957.
(45) Huang, X.; Sevimli, S. I.; Bulmus, V. pH-Labile Sheddable Block Copolymers by RAFT Polymerization: Synthesis and Potential Use as siRNA Conjugates. *Eur. Polym. J.* **2013**, *49* (10), 2895−2905.

(46) Miyata, K.; Christie, R. J.; Kataoka, K. Polymeric Micelles for Nano-Scale Drug Delivery. *React. Funct. Polym.* **2011**, *71* (3), 227−234.
(47) Liechty, W. B.; Peppas, N. A. Expert Opinion: Responsive Polymer Nanoparticles in Cancer Therapy. *Eur. J. Pharm. Biopharm.* **2012**, *80* (2), 241−246.
(48) Torchilin, V. P. Multifunctional Nanocarriers. *Adv. Drug Delivery Rev.* **2012**, *64*, 302−315.
(49) Zhang, L.; Bernard, J.; Davis, T. P.; Barner-Kowollik, C.; Stenzel, M. H. Acid-Degradable Core-Crosslinked Micelles Prepared from Thermosensitive Glycopolymers Synthesized via RAFT Polymerization. *Macromol. Rapid Commun.* **2008**, *29* (2), 123−129.
(50) Lee, I.; Park, M.; Kim, Y.; Hwang, O.; Khang, G.; Lee, D. Ketal Containing Amphiphilic Block Copolymer Micelles as pH-Sensitive Drug Carriers. *Int. J. Pharm.* **2013**, *448* (1), 259−266.
(51) Heffernan, M. J.; Murthy, N. Polyketal Nanoparticles: A New pH-Sensitive Biodegradable Drug Delivery Vehicle. *Bioconjugate Chem.* **2005**, *16* (6), 1340−1342.
(52) Xu, X. W.; Flores, J. D.; McCormick, C. L. Reversible Imine Shell Cross-Linked Micelles from Aqueous RAFT-Synthesized Thermoresponsive Triblock Copolymers as Potential Nanocarriers for "pH-Triggered" Drug Release. *Macromolecules* **2011**, *44* (6), 1327−1334.
(53) Stenzel, M. H. RAFT Polymerization: an Avenue to Functional Polymeric Micelles for Drug Delivery. *Chem. Commun. (Cambridge, U.K.)* **2008**, No. 30, 3486−3503.
(54) Mori, H.; Endo, T. Amino-Acid-Based Block Copolymers by RAFT Polymerization. *Macromol. Rapid Commun.* **2012**, *33* (13), 1090−1107.
(55) Braunecker, W. A.; Matyjaszewski, K. Controlled/Living Radical Polymerization: Features, Developments, and Perspectives. *Prog. Polym. Sci.* **2007**, *32* (1), 93−146.
(56) Moad, G.; Rizzardo, E.; Thang, S. H. Living Radical Polymerization by the RAFT Process - A Third Update. *Aust. J. Chem.* **2012**, *65* (8), 985−1076.
(57) Kurtulus, I.; Yilmaz, G.; Ucuncu, M.; Emrullahoglu, M.; Becer, C. R.; Bulmus, V. A New Proton Sponge Polymer Synthesized by RAFT Polymerization for Intracellular Delivery of Biotherapeutics. *Polym. Chem.* **2014**, *5* (5), 1593−1604.
(58) Guo, R. W.; Wang, X. X.; Guo, C. G.; Dong, A. J.; Zhang, J. H. Facile and Efficient Synthesis of Fluorescence-Labeled RAFT Agents and Their Application in the Preparation of *α*-,*ω*- and *α*,*ω*-End-Fluorescence-Labeled Polymers. *Macromol. Chem. Phys.* **2012**, *213* (17), 1851−1862.
(59) Scales, C. W.; Convertine, A. J.; McCormick, C. L. Fluorescent Labeling of RAFT-Generated Poly(*N*-isopropylacrylamide) via a Facile Maleimide-Thiol Coupling Reaction. *Biomacromolecules* **2006**, *7* (5), 1389−1392.
(60) Vanparijs, N.; Maji, S.; Louage, B.; Voorhaar, L.; Laplace, D.; Zhang, Q.; Shi, Y.; Hennink, W. E.; Hoogenboom, R.; De Geest, B. G. Polymer−Protein Conjugation via a "Grafting to" Approach − a Comparative Study of the Performance of Protein-Reactive RAFT Chain Transfer Agents. *Polym. Chem.* **2015**, DOI: 10.1039/C4PY01224K.
(61) Zhang, Q. L.; Vanparijs, N.; Louage, B.; De Geest, B. G.; Hoogenboom, R. Dual pH- and Temperature-Responsive RAFT-Based Block Copolymer Micelles and Polymer−Protein Conjugates with Transient Solubility. *Polym. Chem.* **2014**, *5* (4), 1140−1144.
(62) Zhang, Q.; Louage, B.; Vanparijs, N.; De Geest, B. G.; Hoogenboom, R. Acid-Labile Thermoresponsive Copolymers That Combine Fast pH Triggered Hydrolysis and High Stability at Neutral Condition: on the Importance of Polymer Architecture. 2014, unpublished results.
(63) Keddie, D. J. A Guide to the Synthesis of Block Copolymers Using Reversible-Addition Fragmentation Chain Transfer (RAFT) Polymerization. *Chem. Soc. Rev.* **2014**, *43* (2), 496−505.
(64) Ferguson, C. J.; Hughes, R. J.; Nguyen, D.; Pham, B. T. T.; Gilbert, R. G.; Serelis, A. K.; Such, C. H.; Hawkett, B. S. Ab Initio Emulsion Polymerization by Raft-Controlled Self-Assembly. *Macromolecules* **2005**, *38* (6), 2191−2204.
(65) Zhang, D. W.; Zhang, H.; Nie, J.; Yang, J. Synthesis and Self-Assembly Behavior of pH-Responsive Amphiphilic Copolymers Containing Ketal Functional Groups. *Polym. Int.* **2010**, *59* (7), 967−974.
(66) Voorhaar, L.; Wallyn, S.; Du Prez, F. E.; Hoogenboom, R. Cu(0)-Mediated Polymerization of Hydrophobic Acrylates Using High-Throughput Experimentation. *Polym. Chem.* **2014**, *5* (14), 4268−4276.
(67) Shi, Y.; van Steenbergen, M. J.; Teunissen, E. A.; Novo, L.; Gradmann, S.; Baldus, M.; van Nostrum, C. F.; Hennink, W. E. *π*−*π* Stacking Increases the Stability and Loading Capacity of Thermosensitive Polymeric Micelles for Chemotherapeutic Drugs. *Biomacromolecules* **2013**, *14* (6), 1826−1837.
(68) Kalyanasundaram, K.; Thomas, J. K. Environmental Effects on Vibronic Band Intensities in Pyrene Monomer Fluorescence and Their Application in Studies of Micellar Systems. *J. Am. Chem. Soc.* **1977**, *99* (7), 2039−2044.
(69) Mosmann, T. Rapid Colorimetric Assay for Cellular Growth and Survival: Application to Proliferation and Cytotoxicity Assays. *J. Immunol. Methods* **1983**, *65* (1−2), 55−63.
(70) Bauer, M.; Lautenschlaeger, C.; Kempe, K.; Tauhardt, L.; Schubert, U. S.; Fischer, D. Poly(2-ethyl-2-oxazoline) as Alternative for the Stealth Polymer Poly(ethylene glycol): Comparison of In Vitro Cytotoxicity and Hemocompatibility. *Macromol. Biosci.* **2012**, *12* (7), 986−998.
(71) van HerkA. M.*Contour*, computer program to calculate reactivity ratios and activation parameters; University of Technology: Eindoven, The Netherlands, 1998
(72) Motokawa, R.; Morishita, K.; Koizumi, S.; Nakahira, T.; Annaka, M. Thermosensitive Diblock Copolymer of Poly(*N*-isopropylacrylamide) and Poly(ethylene glycol) in Water/Polymer Preparation and Solution Behavior. *Macromolecules* **2005**, *38* (13), 5748−5760.
(73) Lutz, J. F.; Weichenhan, K.; Akdemir, O.; Hoth, A. About the Phase Transitions in Aqueous Solutions of Thermoresponsive Copolymers and Hydrogels Based on 2-(2-Methoxyethoxy)ethyl Methacrylate and Oligo(ethylene glycol) Methacrylate. *Macromolecules* **2007**, *40* (7), 2503−2508.
(74) Trinh, L. T. T.; Lambermont-Thijs, H. M. L.; Schubert, U. S.; Hoogenboom, R.; Kjoniksen, A. L. Thermoresponsive Poly(2-oxazoline) Block Copolymers Exhibiting Two Cloud Points: Complex Multistep Assembly Behavior. *Macromolecules* **2012**, *45* (10), 4337−4345.
(75) Battaglia, G.; Ryan, A. J. Bilayers and Interdigitation in Block Copolymer Vesicles. *J. Am. Chem. Soc.* **2005**, *127* (24), 8757−8764.
(76) Canton, I.; Battaglia, G. Endocytosis at the Nanoscale. *Chem. Soc. Rev.* **2012**, *41* (7), 2718−2739.
(77) Lele, B. S.; Leroux, J. C. Synthesis and Micellar Characterization of Novel Amphiphilic A-B-A Triblock Copolymers of *N*-(2-Hydroxypropyl)methacrylamide or *N*-Vinyl-2-pyrrolidone with Poly (is an element of -caprolactone). *Macromolecules* **2002**, *35* (17), 6714−6723.
(78) Miotti, S.; Bagnoli, M.; Ottone, F.; Tomassetti, A.; Colnaghi, M. I.; Canevari, S. Simultaneous Activity of Two Different Mechanisms of Folate Transport in Ovarian Carcinoma Cell Lines. *J. Cell. Biochem.* **1997**, *65* (4), 479−491.
(79) Journo-Gershfeld, G.; Kapp, D.; Shamay, Y.; Kopecek, J.; David, A. Hyaluronan Oligomers-HPMA Copolymer Conjugates for Targeting Paclitaxel to CD44-Overexpressing Ovarian Carcinoma. *Pharm. Res.* **2012**, *29* (4), 1121−1133.
(80) Bast, R. C.; Hennessy, B.; Mills, G. B. The Biology of Ovarian Cancer: New Opportunities for Translation. *Nat. Rev. Cancer* **2009**, *9* (6), 415−428.
(81) Ponta, H.; Sherman, L.; Herrlich, P. A. CD44: From Adhesion Molecules to Signalling Regulators. *Nat. Rev. Mol. Cell Biol.* **2003**, *4* (1), 33−45.